8-20-2019 10:30 AM

# Predicting and preventing traumatic brain injury: A novel computational approach

Kewei Bian
*The University of Western Ontario*

Supervisor
Mao, Haojie
*The University of Western Ontario*

Graduate Program in Mechanical and Materials Engineering
A thesis submitted in partial fulfillment of the requirements for the degree in Master of Engineering Science

# Abstract

Traumatic brain injury (TBI) is a severe health problem for society. Meanwhile, predicting and preventing TBI remains challenging in the field. Peak rotational velocity was demonstrated to be correlated to brain strain responses, and hence could potentially serve as a good predictor for brain injury. Brain strain was influenced by impact direction, deceleration and impact loading curve shapes. Wearing helmets is an effective way to protect the brain from TBI, but there lacks a study on evaluating helmet performance based on both energy absorption and brain strain response, which this study addressed. Interestingly, helmet shell absorbed around half of the energy, followed by interior foams close to impact locations. Facemask also affected brain strain response as it changed both the rigidity and inertia of the helmet.



## Keywords

Traumatic brain injury (TBI), deep brain, strain, rotational velocity, brain strain distribution, pressure, helmet, facemask, energy absorption, helmet dimension change

# Summary for Lay Audience

Traumatic brain injury (TBI) is mostly induced by head motion which is caused by external impact. When the head moves linearly, the skull tends to compress one side of the brain, which induces coup pressure, and compresses the other side of the brain, which induces contre-coup pressure. The high pressure can cause brain damage such as contusion. When the head moves in a rotational manner, the skull shears and stretches the brain tissues because the brain tends to move slower than the skull does. Hence, the neuronal cells in the stretched region will be damaged, which will induce TBI. Generally, there are two ways of biomechanical investigation in protecting the brain: predicting brain injury and preventing brain injury. Different kinds of correlations between kinematic accelerations and TBI were reported to predict TBI. However, the correlations between kinematics and injury lack a fundamental understanding of brain mechanical responses. In this study, the correlation between head rotation and brain strain response was systemically investigated. It was demonstrated that peak rational velocity correlated to brain strain response. Brain strain induced by impact was direction dependent. Axial rotation induced the highest strain, while lateral bending produced the lowest. However, for the deep brain, lateral bending produced the largest brain to the corpus callosum and thalamus. Wearing a helmet is an effective way to protect brain, largely reducing brain strain. The helmet outer shell absorbed around half of the energy, followed by foams close to impact locations. The facemask affected brain strain distribution differently as impact locations changed. The helmet rigidity influenced by facemask was correlated closely to brain strain change induced by facemask.

# Co-Authorship Statement

Chapter 2 (‘A comprehensive investigation of the correlation between head rotation and brain strain’) co-authored by Dr. Haojie Mao is under peer review of Journal of Biomechanics and Modeling in Mechanobiology. Chapter 3 (‘A systemic study of helmet protection mechanism’) co-authored by Dr. Haojie Mao and chapter 4 (‘The role of facemask in brain strain’) co-authored by Yanir Levy, and Dr. Haojie Mao will be sent for publication.

All papers are drafted by Kewei Bian and modified by Dr. Haojie Mao. Moreover, Yanir Levy also helped for draft modifications and data analysis of Chapter 4.

# Acknowledgments

I would like to express my gratitude to Dr. Haojie Mao for his support of my research. I acknowledge Dr. Thomas Jenkyn for his help. I acknowledge Yanir Levy for his help with my research analysis and manuscript modification of chapter 4. I acknowledge that the Canada Research Chairs program and NSERC for support. I also want to thank Dr. Youcai Wu and Dr. Cheng-Tang Wu from LSTC for their help with data analysis.

I acknowledge that Global Human Body Models Consortium (GHBMC) for the support of finite element model.

This study utilized model(s) licensed from Biomechanics Consulting and Research, LC (Biocore), model(s) derived therefrom, or both. The development of those model(s) was made possible by a grant from Football Research, Inc. (FRI) and the National Football League, with input from the NFLPA. The views expressed are solely those of the authors and do not represent those of Biocore, FRI, or any of its affiliates or funding sources [1].

# Table of Contents

# List of Tables

# List of Figures

# List of Appendices

# Acronyms

BrIC: Brain injury criteria

CSDM: Cumulative strain damage measure

CSF: Cerebrospinal fluid

GSI: Gadd severity index

GAMBIT: Generalized acceleration model for brain Injury threshold

HIC: Head injury criterion

MPS: Maximum principal strain

MRI: Magnetic resonance imaging

RIC: Rotational Injury Criterion

TBI: Traumatic brain injury

# Chapter 1

# 1 Introduction

## 1.1 Traumatic brain injury (TBI)

Traumatic brain injury (TBI) is a severe health problem for society and is a challenge in terms of diagnostics and therapeutics [2]. There are 1.6 to 3.8 million patients who suffer from sports-related TBI including concussion in US alone [3]. The severity of the TBI can be classified as moderate-severe TBI, mild TBI and symptomatic TBI [4]. Mild TBI, or concussion, can induce chronic symptoms such as memory loss, cognitive deficits, and balance disturbances [5-7]. Even mild TBI in early life can dramatically increase the risk of brain injury later [8]. Moreover, victims with previous concussion are prone to get another concussion and repeated concussions can lead to long-term brain degeneration [9, 10]. Hence, it is critical to comprehensively understand the biomechanics of TBI and provide better protection methodologies.

## 1.2 The brain & head anatomy

### 1.2.1 Brain anatomy

The brain is a complicated organ with various material properties and anatomical components. The brain can be injured by small deformation, which is different from other body organs like the heart and muscles where deformation may not induce injury [11]. Moreover, the brain could get damaged as brain tissue being stretched under head rotation. The brain consists of the grey and white matter. The grey matter, which is named because of its light grey color [12], includes neuron cells, glial cells, capillaries, neuropil and neuron dendrites. The myelinated axons are included in the white matters which is named because of the color of the myelin. Various components are included in the brain (Figure 1.1). The brainstem, including midbrain, pons, and medulla, is critical to regulate many human behaviors like the auditory, eye movement control, and sleep [13-15]. The cortex is essential to the memory and interference control [16]. Paul et al. reported that the agenesis of the corpus callosum induced the defects of the emotional and social functions [17]. The thalamus is important to the cognitive processing [18]. The basal ganglia plays an

important role in learning and memorizing [19]. The cerebellum is related to movement coordination [20].

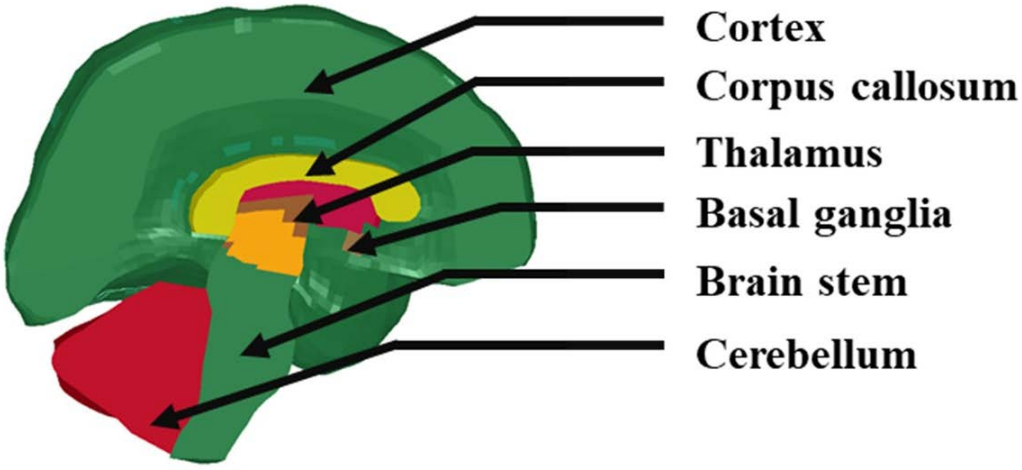


**Figure 1.1 Different brain components.**

### 1.2.2 The skull anatomy

The skull consists of 8 cranium bones and 14 face bones (Figure 1.2). The skull has three layers. The inner and outer layers are made of dense cortical bones, and the medium layer are made of trabecular bones.

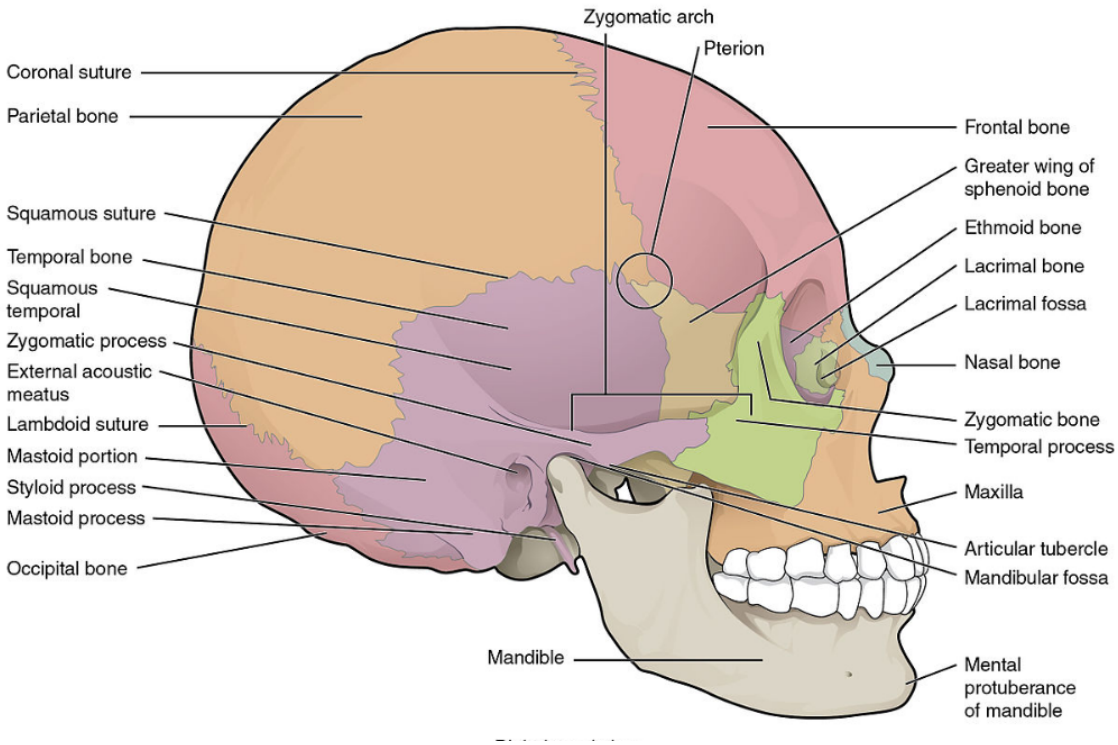


**Figure 1.2 Skull [21] (Adapted from Wikimedia Commons).**

## 1.3 Biomechanical methods to study concussion

To obtain an effective prediction for concussion and hence better protect the brain, understanding the mechanism that induced concussion is critical [22]. Nowadays, concussion is widely investigated using clinical, pathological and biomechanical methods [23]. For biomechanical methods, both experimental methods and finite element (FE) models are extensively used to explore the tissue-level responses of the brain due to impacts [24-26]. These two methods are briefly introduced as follows.

### 1.3.1 Experimental method

#### 1.3.1.1 Laboratory test

In experimental methods, both the video analysis and impact reconstruction were used to get the impact kinematics to the head. The speed at which the players move before and after the impacts can be recorded by cinematographic technology. Two-dimensional velocity can be obtained by the combination of two cameras [27].

The reconstruction test usually includes Hybrid III anthropometric test devices which contain head/neck assembly (dummy) to simulate impacts based on the kinematics being computed by the video analysis [27, 28]. Both linear and rotational accelerations exist during the reconstruction, and the rotational acceleration can be computed based on linear acceleration [27].

#### 1.3.1.2 Concussion criteria based on head kinematics

The linear and rotational kinematics have been demonstrated to induce concussion. There are many laboratories studies establishing the concussion threshold based on the linear and rotational kinematics. Pellman et al. demonstrated that concussive players experienced peak linear acceleration of 98 ± 28 g [27]. The peak linear acceleration ranged from 61 to 144 g was reported by Zhang et al. [29]. Margulies and Thibault suggested the threshold of 1,600 rad/s$^2$ based on the primate model [30]. Moreover, in terms of linear and rotational kinematics, many brain injury metrics were used to quantify brain injury. The currently used brain injury metrics which were based on head acceleration includes Head Injury Criterion (HIC), Rotational Injury Criterion (RIC), Generalized Acceleration Model for Brain Injury Threshold (GAMBIT), and Brain injury Criteria (BrIC) [31-35]. Although impact kinematics can induce brain injury, it should be noted that kinematics cannot directly explain why the brain is injured.

### 1.3.2 Finite element analysis and brain response

#### 1.3.2.1 Finite element analysis

The FE analysis is a numerical analysis that can be used to predict mechanics-related head damage [11]. The brain-damage-related responses like brain strain and pressure can be reflected by FE model under simulated impact. The FE model, which is generated based on head geometry which is developed from magnetic resonance imaging (MRI) scans[36], consists of elements with specific dimensions to represent specific head components. Wayne State University brain injury model (WSUBIM) was developed as early as in 1990's. The latest WSUBIM model contains 281,800 nodes and 314,500 elements [37]. In 1997, Kang et al. developed the Université Louis Pasteur (ULP) human head model [38]. Totally, the model contained 13,208 elements, involving the skull, falx, tentorium,

subarachnoid space, scalp, cerebrum, cerebellum and brainstem. The skull' s inner and outer surfaces were digitalized based on male adult skull. The Lagrangian formulation was used in cerebrospinal fluid (CSF), and the elastic material which was validated by the test was used in brain-skull interface [39]. In 2002, Kleiven and Hardy reported the model called Kungliga Tekniska Högskolan (KTH) [40]. The model contained 18,400 elements, and some key features such as the scalp, skull, brain, meninges and CSF were included. Different types of material models such as homogeneous, isotropic and non-linear material models were used in KTH model [39]. In 2003, Takhounts and Eppinger created simulated injury monitor (SIMon) model, which represented 50th percentile male [41]. The skull was defined as the rigid body, while the other parts were regarded as deformable parts [39]. In 2013, the Global Human Body Models Consortium (GHBMC) FEM was developed by Mao et al [36]. The GHBMC head model is a detailed head model containing key features of brain including the cerebrum, cerebellum, brainstem, corpus callosum, ventricles, and thalamus. The model was validated against intracranial pressure data, brain displacements, nasal impact and frontal horizontal impact [36].

#### 1.3.2.2 Injury tolerance at tissue level

Brain strain is mostly used tissue-level response in predicting TBI or concussion. There were studies reporting the range of 0.19-0.21 strain for mild TBI [25, 29] based on the whole brain response. The strain thresholds are different for various brain components. For the corpus callosum, the strain tolerance was reported as 0.28 and 0.31 [42, 43], and the tolerance for 50% likelihood ranged from 0.15 to 0.21 [25, 29, 42]. For the thalamus, the strain tolerance was reported as 0.26 to 0.38 [42, 44]. There are many factors that can influence brain strain. Zhao et al. and Yoganandan et al. reported that the shape of impact curves can affect brain strain [45, 46]. Post et al. demonstrated that the magnitudes and durations of impact curves can influence brain strain [47]. Zhang et al. and Elkin et al. reported that the impact locations can also influence brain strain [48, 49]. However, there lacks a systemic study investigating the correlation between head kinematics and brain strain, especially how head rotation at various directions could affect the whole brain and deep brain structures.

## 1.4 Helmet

### 1.4.1 The effectiveness of the helmet

Wearing helmet (Figure 1.3) is regarded as an effective way to protect the head. When helmets were mandatory in American football events, brain-injury-related deaths were reduced from around 150 in 1965-1974 to 25 in 1985-1994 [50]. Moreover, Rowson et al. reported that using helmet could reduce the occurrence of concussion [51]. Trotta et. al reported that helmet could decrease 65% risk of brain injury from cycling [52]. Viano et al. reported that updated helmet design could reduce brain injury risk [53]. Karus et al. demonstrated that a well-designed hockey helmet can decrease 8.3 head injuries per 100 games to 3.8 head injuries per 100 games [54]. There were different kinds of helmets being optimized to protect brain [53]. As expected, the performance of helmet in brain injury risk reduction varied by different helmets [28].


**Figure 1.3 Riddell helmet with facemask [55] (Adapted from Wikimedia Commons).**

### 1.4.2 Helmet performance evaluation

There are different kinds of standards to evaluate the effectiveness of helmet. The standards include linear acceleration of dummy head with the pass/fail acceleration of approximately

250 g [56],Gadd Severity Index (GSI) and Head Injury Criterion (HIC), which were all established based on dummy head kinematic response [57-59]. However, there are several limitations for the head kinematic-based helmet performance evaluation. First, The dummy head and neck are stiffer than those of real humans [60], which could induce higher kinematics responses than actual responses. Second, the head motion data was difficult to collect as Joodaki et al. reported that the kinematic responses of dummy head were highly dependent on the relative motion between the helmet and the head [61]. Compared to head kinematics, brain strain is regarded as a good brain injury predictor because brain strain can cause brain injury directly, as neurons could get damaged as brain tissues were stretched [62]. To evaluate helmet performance in terms of reducing injury, it is necessary to understand ways that how a helmet can reduce the strain.

### 1.4.3 Facemask

The facemask (Figure 1.7) is a necessary part of a football helmet because it can prevent players from face injury during sports. However, as helmets were tested without facemasks based on the current standard, the effect of a facemask on brain injury is unclear. Breedlove et al. reported that the inclusion of facemask itself increased the head acceleration by up to 36% from the dummy, which may increase brain injury risk [63]. A similar result was also demonstrated by Rush et al [64]. Although Rowson et al. found the facemask reduced head kinematics, whether the facemask influenced brain injury is still unknown [65]. As brain strain is highly correlated to brain injury, it is necessary to demonstrate the influence of the facemask to brain strain response.

## 1.5 Brain biomechanics to neuronal degeneration

Experimental studies especially those from animal studies and human subjects demonstrated that significant axonal tract damage [66-68], cell body damage [69], and astrocyte damage [70] occurred for healthy subjects undergoing blunt impacts. The remaining question is what kinds of brain mechanical responses are responsible for such damage. After decades of research, brain strain has been proven to induce axonal changes [62], neuronal loss [71], as well function-related neural electricity dysfunction [72]. These studies usually involved an in vitro device that could directly stretch brain tissues. The

contribution of strain to brain damage may also explain the region-specific, heterogeneity of brain damage observed during experiments. Compared to strain which is a deviatoric mechanical response, pressure as a dilatational response is less studied in terms of its contribution to concussion. There is no direct link between impact-induced brain pressure and neuronal damage. However, it was supported that the classical coup (positive) and contre-coup (negative) pressures were related to brain damage like contusion [11]. Also, in vitro studies designed to mimic blast wave conditions demonstrated that fluid-transferred high pressure caused neuronal cell, axon, and astrocyte damage [73, 74]. Hence, despite the lack of direct links between blunt-impact relevant pressure and brain injury, pressure response was also analyzed in this study.

## 1.6 Objective of this study

To better understand concussion biomechanics and hence provide more efficient protection, it is necessary to understand how the brain responds during impacts and how protective gears like helmets reduce such responses. Hence, the objectives of the research were to: 1) systematically evaluate how kinematics correlated to brain strain under different impact directions, acceleration magnitudes, durations, decelerations, as well as loading curves with different shapes, mimicking complex real-world impacts 2) investigate the how helmet can protect the brain with the quantification of brain strain and pressure, and 3) evaluate how facemask influences brain strain and pressure.

## 1.7 Thesis structure

Chapter 2 describes the correlation between head kinematics and brain strain responses. A well-defined FE head model was impacted under concussive acceleration loading. The correlation between peak rotational velocity and brain strain distribution was investigated. The direction-dependent effect on the whole brain and deep brain components were also evaluated. Moreover, this chapter describes how deceleration, loading curves with different shapes and linear acceleration affected brain strain.

Chapter 3 describes the mechanism of helmet to protect brain. Compared to the bare head, how the helmet affected brain strain response was evaluated. This chapter also includes impact energy absorption effect of different helmet components.

Chapter 4 evaluates the influence of facemask to brain response. An impactor was used to hit six locations of the helmeted head & neck FE models, with and without facemask. The helmet dimension change (before and after impact) induced by facemask was used to correlated to the brain response difference that facemask produced,

Chapter 5 concludes the main findings this study, lists the limitations and introduces the future study. Chapter 5 also summarizes the significance and novelty of this study.

# Chapter 2

# 2 A comprehensive investigation of the correlation between head rotation and brain strain

There lacks a comprehensive understanding of the correlation between head kinematics and brain strain especially deep-brain strain, partially resulting in the difficulty of choosing appropriate brain injury metrics. Hence, we simulated 76 impacts that were focused on concussion-relevant rotational kinematics and evaluated the cumulative strain damage measure (CSDM) that could represent brain strain distribution.

## 2.1 Introduction

There are 1.6 to 3.8 million sports-related Traumatic Brain Injuries (TBIs) including concussions in US alone [3]. Concussion induces symptoms such as memory loss, cognitive deficits, and balance disturbances [5, 6]. Nowadays, concussion is widely investigated using clinical, pathological and biomechanical methods [6, 23]. For biomechanical methods, both experimental methods and finite element (FE) models are extensively used to explore the tissue-level responses of the brain due to impacts [25, 26, 75].

Concussion has been demonstrated to be related to linear and rotational head kinematics. Pellman et al. reported that concussive players experienced peak linear acceleration of 98 ± 28 g [27]. The peak linear acceleration ranged from 61 to 144 g [29]. Margulies and Thibault suggested the threshold of 1,600 rad/s$^2$ based on a primate model [30]. Rowson et al. published the thresholds of concussion as 5,260, 5,281, 6,383, 6,945 and 7,483 rad/s$^2$ for the concussion risk of 10%, 25%, 50%, 75% and 90%, respectively [76]. Most concussive cases happen with the peak rotational acceleration around 5 krad/s$^2$ (Figure 2.1a) [23, 27, 76-79]. For impact durations, Greenwald et al. reported that 95% of impacts happened between 5.5 and 13.7 ms [80]. Rowson et al. also recorded the average duration of 14 ms for helmeted head impacts [81]. Based on the above data, systematically investigating brain responses induced by reported head kinematics related to concussion will be critical.

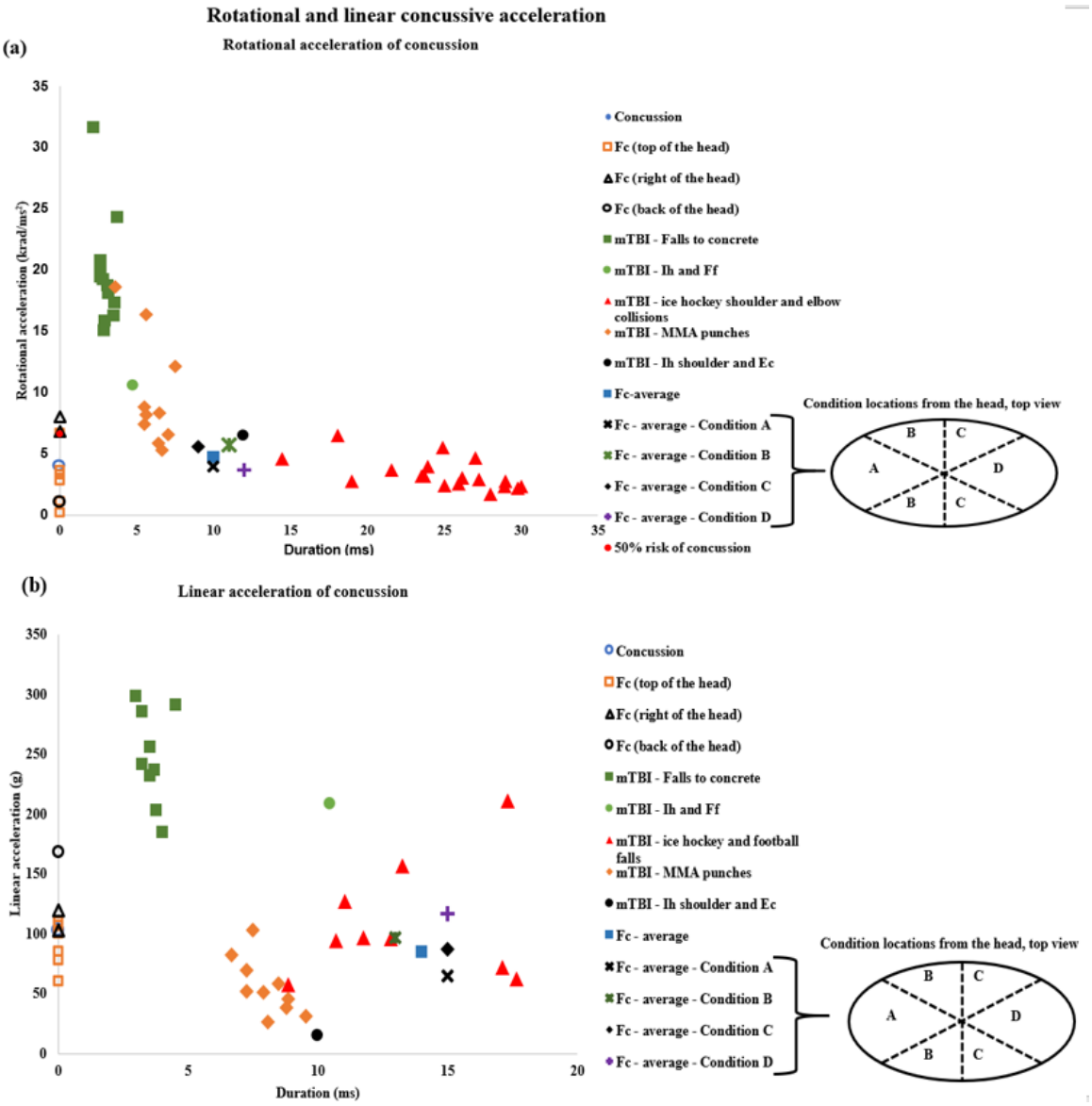


**Figure 2.1: Rotational and linear accelerations that cause concussion. (a) literature-reported linear acceleration of concussion; (b) literature-reported rotational acceleration of concussion *[23, 27, 76-79, 82]*. Fc: football concussion. Ih: ice hockey. Ff: football fall. Ec: elbow collision. mTBI: mild traumatic brain injury. MMA: mixed martial art.**

The brain response is crucial for predicting TBI including concussion. Kleiven summarized 10 predictors that were widely used for predicting TBI. The predictors relevant to brain responses include strain, strain rate, product of strain and strain rate, cumulative strain damage measure (CSDM), strain energy density, maximum pressure, magnitude of

minimum pressure and von Mises effective stress [25]. The use of maximum principal strain (MPS) was suggested by Thibault et al. and Bain et al. [62, 83]. Von Mises stresses and strain energy were used as the predictors by Shreiber et al. [84]. The product of strain and strain rate was suggested by Viano and Lovsund [85], King et al. [86], and Zhang et al. [29]. The CSDM was suggested as the predictor of brain responses by Takhounts et al. and Kimpara et al. [31, 32, 41, 87].

Brain strain is of significance in predicting TBI or concussion. There are studies reporting the range of 0.19-0.21 for mild TBI [25, 29] based on the whole-brain strain. However, it is accepted that deformation produced by impact can cause different symptoms in various brain areas [59], highlighting the importance to investigate regional responses. The corpus callosum was reported to be related to the abnormal interhemispheric functional connectivity and motor impairments [88]. Some concussion cases were reported to be related to the thalamus and basal ganglia [89]. The thalamus can transmit the information throughout the brain and join the communication with other brain regions, involving the multifunctional global pathways [90]. In addition, the basal ganglia is critical for learning and memorizing [19]. Knowing the brain region-dependent functions, researchers have conducted studies on the responses of different brain components such as the corpus callosum, thalamus and brainstem under impacts [25, 42, 47]. For the corpus callosum, the strain tolerance was 0.28 and 0.31 [42, 43], and the tolerance for 50% likelihood ranged from 0.15 to 0.21 [25, 29, 42] For the thalamus, the strain tolerance ranged from 0.26 to 0.38 [42, 44]. The whole-brain and deep-brain components may response differently under the same impact, as their thresholds were different, which highlighted the importance of investigating how impacts affect the whole and the deep-brain.

With the understanding that brain strain directly connects to brain damage, while head kinematics are currently used when developing protection gear, one major challenge is to systematically investigate the correlations between head kinematics and brain strain under complex impact scenarios. Below we reviewed commonly used kinematic magnitudes, impact directions, and linear/rotational impacts. We also reviewed rotational acceleration curve shapes and rotational deceleration.

Different impact locations induced various brain responses [48, 49] Zhang et al. simulated frontal and lateral impacts to the brain and found that lateral impact produced higher shear stress than frontal impact did [49]. Elkin et al. reported that the MPS and CSDM of the rear eccentric impacts were higher than those from other impacts [48]. Hernandez et al. reported that the corpus callosum had high correlation to lateral impacts [91]. However, impact direction is not equal to head kinematics. For example, a lateral impact to the face can induce a combination of head lateral bending and axial rotation. Hence, evaluating the influence of individual rotational direction, such as flexion/extension, lateral bending, and axial rotation, is beneficial to understand concussion.

The effects of linear and rotational kinematic on brain responses have been studied. King et al. found that brain motion (± 1 mm) induced by linear acceleration was less than that induced by rotational acceleration [86] (± 5 mm). Zhang et al. reported that linear acceleration greatly affected intracranial pressure, and rotational acceleration greatly influenced shear stress [29]. Kleiven also found that rotational kinematics had a higher correlation to the strain than translational kinematics did [25]. Elkin reported that there was a strong correlation between rotational kinematics and strain [92]. Moreover, Post et al. found that the combination of linear and rotational acceleration could induce higher MPS than the pure rotational acceleration did within the first 10 ms of impacts [47]. Hence, investigating impacts with various combinations of linear and rotational kinematics is helpful to provide more evidence on the effect of rotational impacts.

Deceleration exists during the whole impact of football game [93]. Both acceleration and deceleration can cause concussion [93]. The process of deceleration was reported in the cadaver tests [94]. The deceleration loading curves were also studied. However, although brain responses to acceleration are widely studied [47, 78], brain responses to deceleration are not known, and need to be investigated.

The head kinematic loading curves consist of different shapes [75, 81]. The different shapes of the impact curves result in different brain responses. Zhao et al. reported that the shape variation influenced the magnitude of brain strain [46]. Post et al. demonstrated that MPS and Von Mises stress were influenced by the occasion of when the loading curves will

reach to the peak value, and the curves with longer duration before reaching the peak induced higher brain strain [75]. Yoganandan et al. also revealed that brain strain was dependent on the load curve shapes [45]. Hence, it is necessary to investigate the effects of curve shapes on the brain responses.

In this study, we comprehensively investigated the correlations between head kinematics and brain responses. For brain responses, we focused on the CSDM [32, 57, 95] to correlate to diffuse brain injuries because CSDM represents the proportion of brain volumes exceeding specific strain level to the whole brain volume, while peak strain or peak strain rate were not included. We conducted a total of 76 simulations to understand brain strain under various impacts. Our data revealed how rotational velocity correlated to the CSDM, under different impact directions, acceleration magnitudes, durations, decelerations, as well as loading curves with different shapes. Our data also showed how correlation was further changed when organizing impacts into different groups based on impact direction. Additionally, our data included rotational deceleration, which hasn't been addressed in existing kinematics-based injury threshold.

## 2.2 Method

### 2.2.1 Finite element model

The Global Human Body Model Consortium (GHBMC) head model including brain components such as the cerebellum, brainstem, corpus callosum, basal ganglia and thalamus was used to evaluate brain responses (Figure 2.2a and 2.2b) [36, 96]. The model contained 270,552 elements consisting of beam, shell and solid elements, 183,795 nodes and 62 components [36]. The element size was around 3 mm in general. The shell elements had the minimum aspect ratio of 7.45, maximum warpage value of 69.8 and minimum Jacobian number of 0.43. The solid elements had the aspect ratio below 8, maximum warpage value of 96.9 and minimum Jacobian number of 0.40. Linear visco-elasticity material was used for both the gray matter and the white matter. The skull was defined as an elastic-plastic material with inner table, outer tale, and trabecular layer [36]. More information about model material properties can be found in Appendix A. The model was validated against intracranial pressures and brain displacements [97-99]. Ls-PrePost

version 4.3 was used for the simulation preparation and analysis [100]. Ls-Dyna R901was used to calculate simulations [101]. The timestep of the simulation was 0.12 ms.

### 2.2.2 Description of linear and rotational curves

The linear and rotational acceleration time history curves were imposed to the center of gravity of the GHBMC head model. The sinusoidal curves were used for the linear and rotational impacts. To simulate the concussive case, we defined 32 pure rotational impact simulations with two peak magnitudes (2.5 and 5 krad/ms$^2$) based on Figure 2.1, and four durations levels (5, 10, 15 and 20 ms) with additional 10 ms afterwards respectively (Figure 2.2c). All these two magnitudes and four levels were applied to four impact directions to evaluate the effect of different impact directions on brain strain response, yielding 32 cases. For four combined linear and rotational cases, the rotational acceleration curve with peak magnitude of 5 krad/ms$^2$ and duration of 10 ms was combined with the linear acceleration curve with peak magnitude of 50 g and duration of 10 ms to explore brain strain to evaluate the effect of linear acceleration on brain strain response . For 12 cases related to rotational deceleration, the peak rotational acceleration of 5 krad/ms$^2$ and positive duration of 10 ms was used, combined with four levels of deceleration duration (10, 20, 30 and 40 ms) (Figure 2.2d), providing the exact same rotational velocity and same duration when studying deceleration effect. These four levels of deceleration applied to three impact directions (lateral bending, extension and axial rotation), yield 12 cases. For 28 cases related to curve shapes, seven curve shapes (Figure 2.2e and 2.2f) beside sinusoidal shape were applied in four impact directions. The curve shapes included rectangle, trapezium and triangle, all with the peak acceleration of 5 krad/s$^2$ and the acceleration duration 10 ms. Two kinds of trapezoid curves with the peak acceleration occupying the 1/3 and 2/3 of the acceleration duration respectively (Figure 2.2e) were selected. Four kinds of the triangle curves were applied with the peak acceleration point reaching at the start, 1/3, 2/3 and the end of the whole acceleration duration (Figure 2.2f).

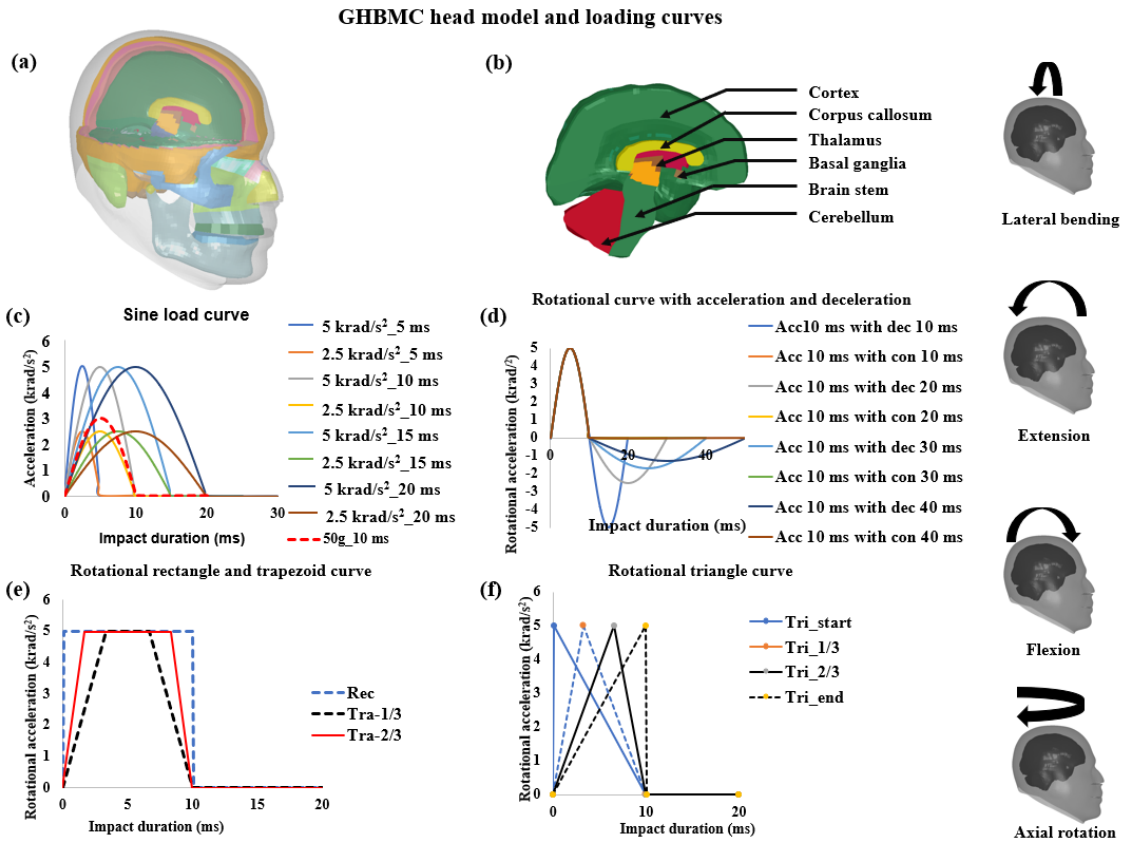


**Figure 2.2 The Global Human Body Model Consortium (GHBMC) head model and loading curves. (a) the head model; (b) the brain model; (c) Sine load curve; 5 krad/s$^2$ indicates the peak acceleration was 5 krad/s$^2$, and 5 ms indicates impact duration. (d) the rotational load curve with acceleration and deceleration; Acc indicates acceleration, and dec indicates deceleration. (e) Rotational rectangle and trapezoid load curve; Rec indicates rectangle curve; Tra-1/3 indicates trapezoid curve with the peak acceleration occupying 1/3 of the duration; Tra-2/3 indicates trapezoid curve with the peak acceleration occupying 2/3 of the duration. (f) Rotational triangle curve; Tri-start indicates triangle curve peaking at the start of the curve; Tri-1/3 indicates triangle curve peaking at the 1/3 of the curve; Tri-2/3 indicates triangle curve peaking at the 2/3 of the curve; Tri-end indicates triangle curve peaking at the end of the curve.**

### 2.2.3 Analysis method

Both MPS contour and CSDM value were used to demonstrate the simulation result. The results of the CSDM20, which represents the percentage of the elements for which the strain is higher than 0.20, were primarily presented to for analysis while the results of other CSDM levels were listed in the Appendix B, because 0.20 was suggested as a strain threshold of concussion [25, 29]. The relative mean difference (RMD) (Eq 2.1) [64] was used to show the difference between linear-with-rotational and rotational-only groups, indicating the effect of linear motion on brain strain distribution. The CSDM difference (Eq 2.2) was used to show the difference between with-deceleration group and without-deceleration group. R-squared regression analysis was used to analyze the correlation between the CSDM values and velocities.

$$\boldsymbol{RMD = \frac{CSDM.LR - CSDM.R}{CSDM.R}} \qquad \textbf{Eq 2.1}$$

Where RMD is Relative mean difference, CSDM.LR is CSDM from impacts with both linear and rotational accelerations, CSDM.R is CSDM from impacts with rotational acceleration.

$$\boldsymbol{CSDM\ difference = \frac{CSDM.w.d - CSDM.wo.d}{CSDM.wo.d}} \qquad \textbf{Eq 2.2}$$

Where CSDM.w.d is CSDM from impacts with rotational deceleration, CSDM.wo.d is CSDM from impacts without rotational deceleration.

## 2.3 Results

### 2.3.1 Brain strain distribution due to rotational impact

For the whole brain, axial rotation induced the largest MPS distribution, followed by extension & flexion and lateral bending (Figure 2.3). For an impact duration of 10 ms, the CSDM20 from axial rotation was calculated as 0.41, followed by the CSDM20 from flexion and extension (Figure 2.4a). The extension & flexion had a similar result, with the CSDM20 0.23. The CSDM20 result of lateral bending was the lowest (Figure 2.4a) at 0.16.

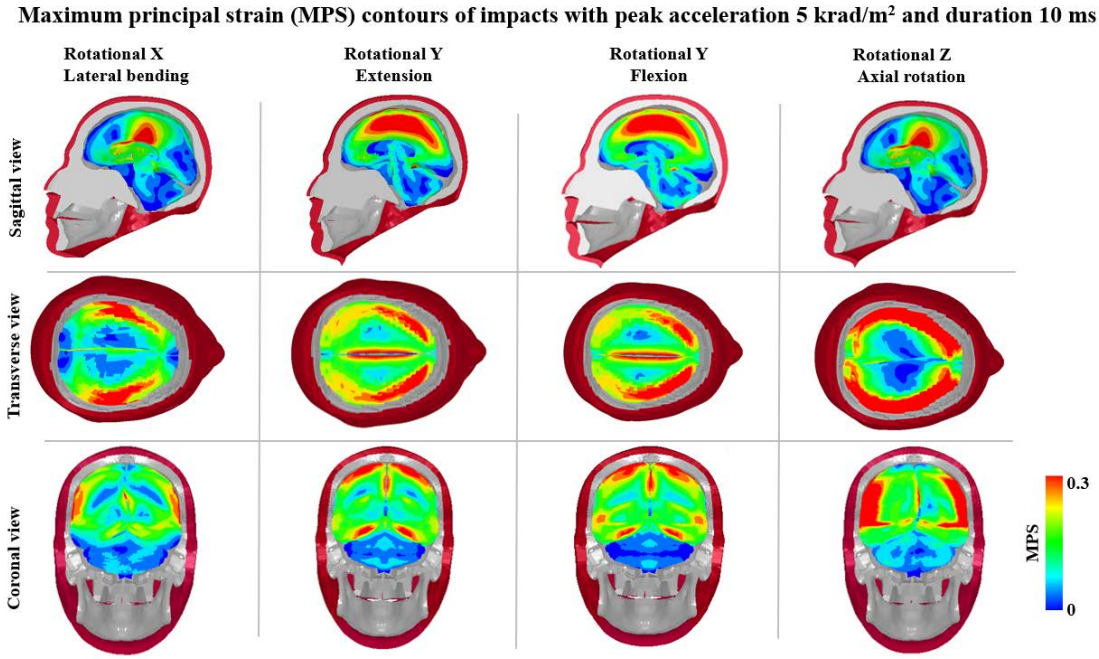


**Figure 2.3 Maximum principle strain (MPS) contours of impacts with peak acceleration 5 krad/s$^2$ and duration 10 ms. Three views (sagittal, transverse and coronal) of the MPS contours were plotted with the range between 0 and 0.3.**

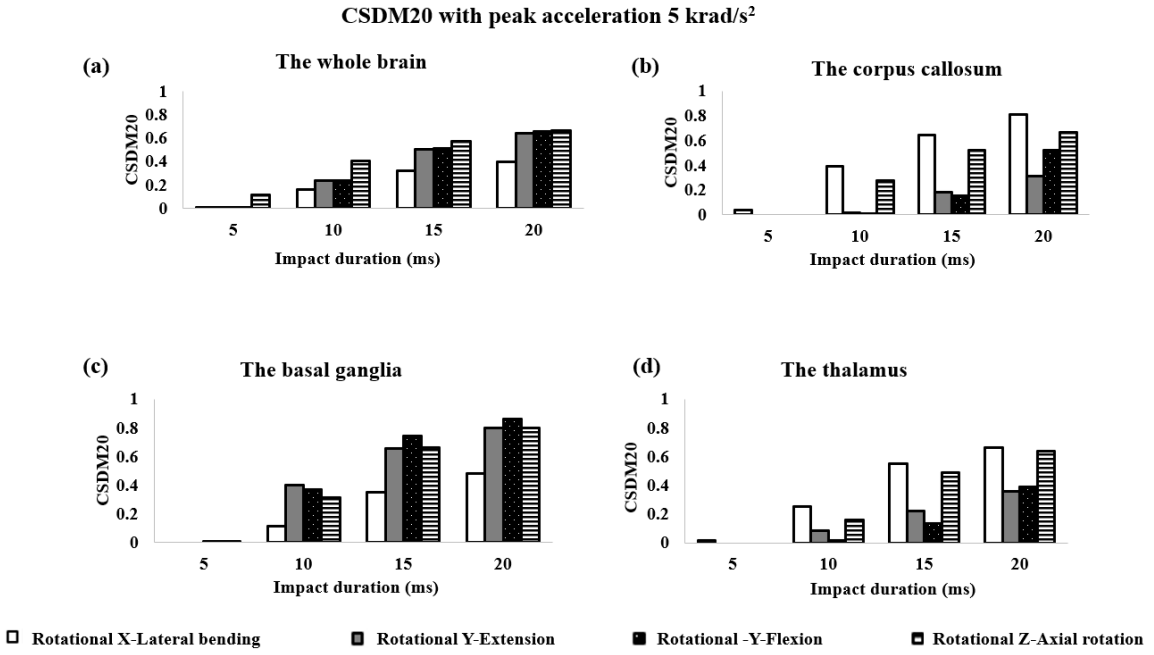


**Figure 2.4 CSDM20 of different brain regions under different impacts. (a) CSDM20 for the whole brain; (b) CSDM20 for the corpus callosum; (c) CSDM20 for the basal ganglia; (d) CSDM20 for the thalamus.**

For the corpus callosum, lateral bending produced highest CSDM values among all the CSDM levels followed by the CSDM values induced by axial rotation. Flexion and extension produced the lowest CSDM values (Figure 2.4b). With impact duration 10 ms, CSDM20 value produced by lateral bending and axial rotation were 0.39 and 0.28, respectively. Mostly, the CSDM20 values produced by extension were higher than those produced by flexion except for the condition of impact duration 20 ms.

For the basal ganglia, overall, the CSDM values produced by flexion and extension were highest, followed by those produced by axial rotation and lateral bending (Figure 2.4c). The CSDM values induced by flexion and extension were slightly different depending on CSDM levels. For the CSDM20 within impact duration 10 ms (Figure 2.4c), the values induced by flexion and extension, axial rotation and lateral bending were 0.4, 0.37, 0.31 and 0.11 respectively.

For the thalamus, interestingly, lateral bending, which produced the lowest CSDM within the whole brain, induced the largest CSDM in the deep-brain region (Figure 2.4d), followed by axial rotation, flexion and then extension. With impact duration of 10 ms, lateral bending, axial rotation, extension flexion produced CSDM20 of 0.25, 0.16. 0.08 and 0.01.

### 2.3.2 CSDM relative mean difference (RMD) between impacts of the combination of linear and rotational accelerations and pure rotational acceleration

Generally, except for the case with combined lateral bending and translational motion, the RMD that indicates the relative mean difference didn't increase obviously, only with the increase within 1% (Table 2.1). Even for the case with combined lateral bending and translational model, the absolute differences of the CSDM were less than 0.03.

**Table 2.1 CSDM relative mean difference (RMD) for impacts with combined of linear and rotational acceleration and impacts with rotational acceleration**

| CSDM level | 0.1 | 0.15 | 0.2 | 0.25 | 0.3 |
|---|---|---|---|---|---|
| Linear X and flexion (Rotational -Y) vs flexion | 0.14% (0.7409 vs 0.7399) | 0.29% (0.4687 vs 0.4673) | 0.74% (0.2366 vs 0.2348) | 0.40% (0.0930 vs 0.0926) | 0.57% (0.0396 vs 0.0394) |
| Linear -X and extension (Rotational Y) vs extension | 0.08% (0.7254 vs 0.7249) | 0.37% (0.4597 vs 0.4580) | 0.66% (0.2371 vs 0.2355) | 0.85% (0.0963 vs 0.0955) | 0.31% (0.0383 vs 0.0382) |
| Linear Y and lateral bending (Rotational X) vs lateral bending | 2.67% (0.6017 vs 0.6182) | 7.09% (0.3361 vs 0.3617) | 8.78% (0.1471 vs 0.1613) | 12.98% (0.0565 vs 0.0649) | 25.44% (0.0180 vs 0.0241) |
| Linear Y and axial rotation (Rotational Z) vs axial rotation | 0.67% (0.8808 vs 0.7955) | 0.91% (0.5922 vs 0.5868) | 0.33% (0.4066 vs 0.4052) | 0.41% (0.2671 vs 0.2682) | 0.75% (0.1678 vs 0.1690) |

### 2.3.3 The effect of deceleration

Overall, a large difference existed when deceleration was considered. Rotational deceleration in axial rotation model produced highest changes to the CSDM among all three directions (27% increase of CSDM20) (Figure 2.5). The CSDM difference with other

strain levels were listed in Appendix C. Rotational deceleration in lateral bending mode and extension mode also affected CSDM. Interestingly, deceleration reduced CSDM values when deceleration durations were short (≤ 10 ms for all loading modes and ≤20 ms for the extension loading mode) and increased the CSDM values when deceleration durations were long (≥ 20 ms for lateral bending and axial rotation loading modes, ≥ 30 ms for extension loading mode). The result of other directions presented the similar result (Appendix C)

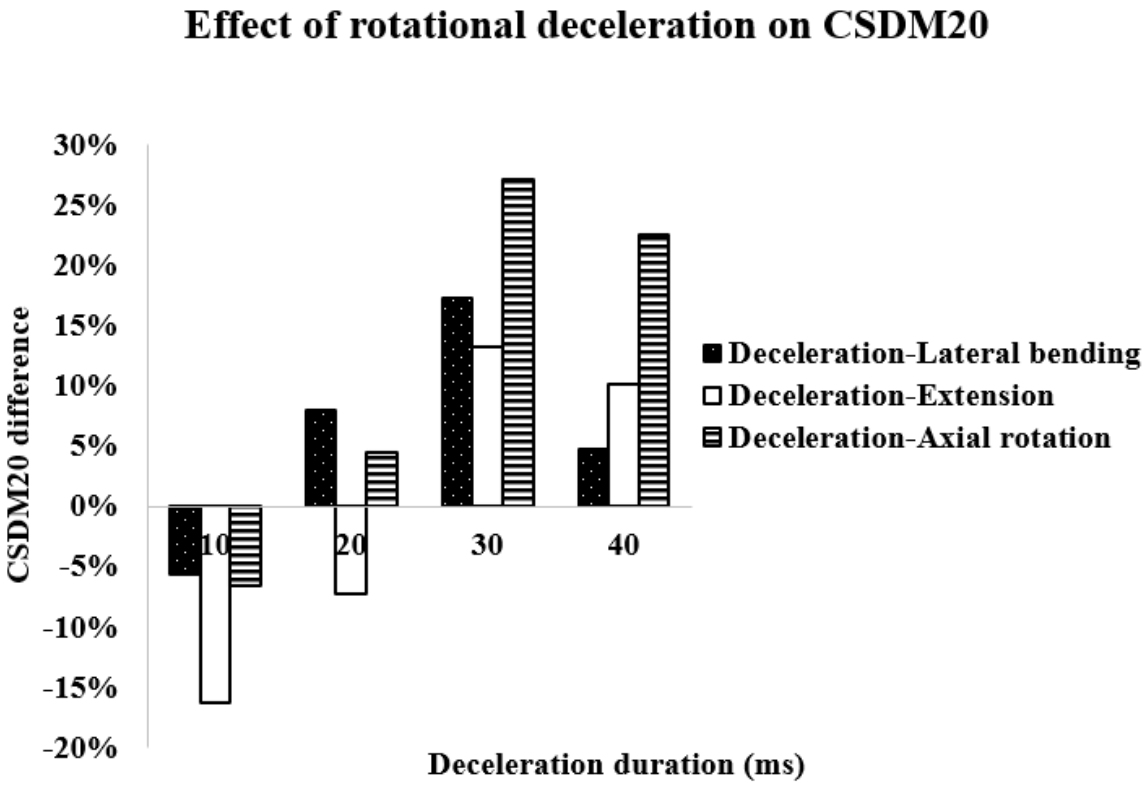


**Figure 2.5 Effect of rotational deceleration on CSDM20**

### 2.3.4 The effects of loading curves with different shapes

The rectangular shape loading curves induced the highest CSDM valude, with CSDM20 of 0.62, 0.55 and 0.37 under axial rotation, flexion & extension and lateral bending respectively. (Figure 2.6). The trapezoid curve with the peak acceleration occupying 2/3 of duration caused the second largest strain distribution (Figure 2.6). Axial rotation induced

the CSDM20 of 0.54, which was the largest among all impacts. The impacts with the trapezoid curve with peak acceleration occupying 1/3 of the duration produced the third largest the CSDM20 values, with the CSDM20 of 0.43 induced by the axial rotation, CSDM20 of 0.27 generated by flexion and extension, and the CSDM20 of 0.18 under lateral bending (Figure 2.6). The CSDM20 values from the sine-curve loading and from the trapezoid-curve loading with peak acceleration of 1/3 of the duration were similar (Figure 2.6). The lowest CSDM20 results were from the triangular curves (Figure 2.6). Among the four triangle shapes, overall the CSDM values were close. However, the triangle-curve loading with acceleration peaking at 2/3 of duration produced the highest value, while the triangle-curve loading with acceleration peaking at the beginning generated the lowest (Figure 2.6).

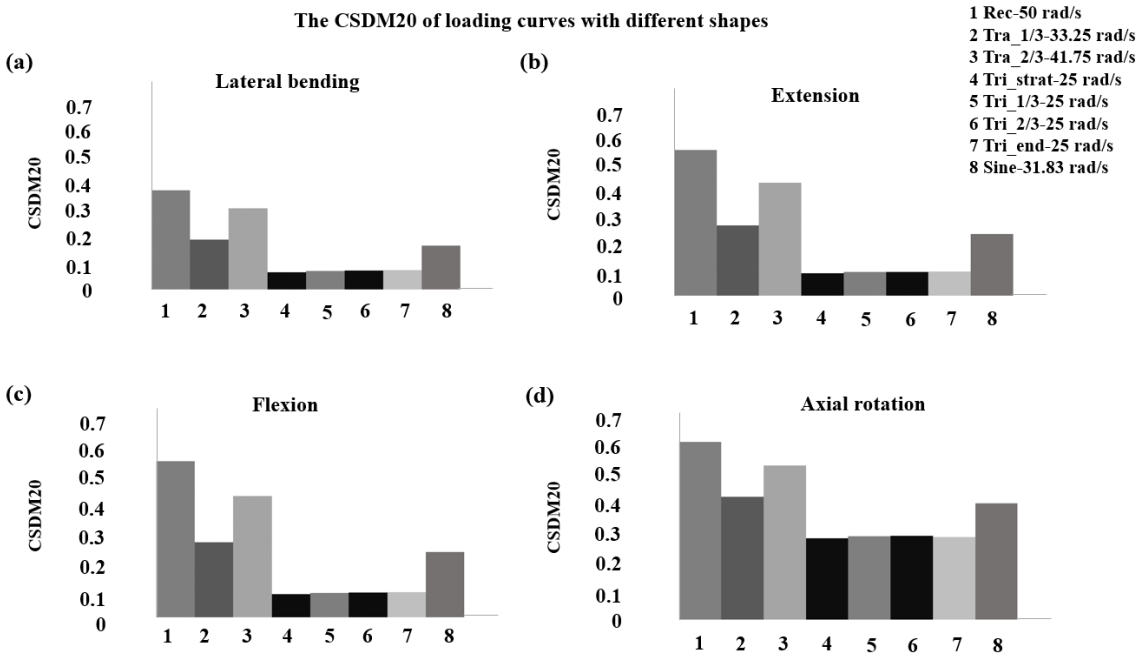


**Figure 2.6 The CSDM20 of impacts with loading curves with different shapes. (a) the CSDM20 of load curve with different shapes under lateral bending. (b) the CSDM20 of load curve with different shapes under extension. (c) the CSDM20 of load curve with different shapes under flexion. (d) the CSDM20 of load curve with different shapes under axial rotation. For the legend, Rec indicates rectangle curve, and its integrated velocity was 50 rad/s; Tra-1/3 indicates trapezoid curve with the peak impulse occupying 1/3 of the duration, and its integrated velocity was 33.25**

**rad/s; Tra-2/3 indicates trapezoid curve with the peak impulse occupying 2/3 of the duration, and its integrated velocity was 41.75 rad/s; Tri-start indicates triangle curve peaking at the start of the duration, and its integrated velocity was 25 rad/s; Tri-1/3 indicates triangle curve peaking at the 1/3 of the duration, and its integrated velocity was 25 rad/s; Tri-2/3 indicates triangle curve peaking at the 2/3 of the duration, and its integrated velocity was 25 rad/s; Tri-end indicates triangle curve peaking at the end of the duration, and its integrated velocity was 25 rad/s.**

### 2.3.5 Correlation between rotational velocity and the CSDM

Correlations between the CSDM and kinematics are shown in Figure 2.7. For sine-shape rotational velocity loadings with different peak accelerations (2.5 and 5 krad/s$^2$) and different impact durations (5, 10, 15 and 20 ms), velocities highly correlated with CSDM20 with $R^2$ all above 0.94 for four directions (lateral bending, extension, flexion, and axial rotation) groups (Figure 2.7a). For other CSDM levels, $R^2$ values of most cases were above 0.9 (Appendix D). When considering different shapes (Figure 2.3c and 2.3d), $R^2$ values also reached to very high numbers above 0.99 for four direction groups (Figure 2.7c), while the correlation between the CSDM20 and peak acceleration was not obvious under this condition (Figure 2.7d). Mixing all directions and shapes as well as peak accelerations and durations into one group, $R^2$ values were 0.72, 0.80, 0.78, 0.76, and 0.70 for the CSDM10, CSDM15, CSDM20, CSDM25, and CSDM30 respectively (Figure 2.7e). However, for the correlation between CSDM20 and acceleration, the $R^2$ was around 0.40 under different impact directions (Figure 2.7b). $R^2$ values were 0.30, 0.34, 0.36, 0.30 and 0.30 under the correlation between the CSDM (with different strain level) and acceleration (Figure 2.7f).

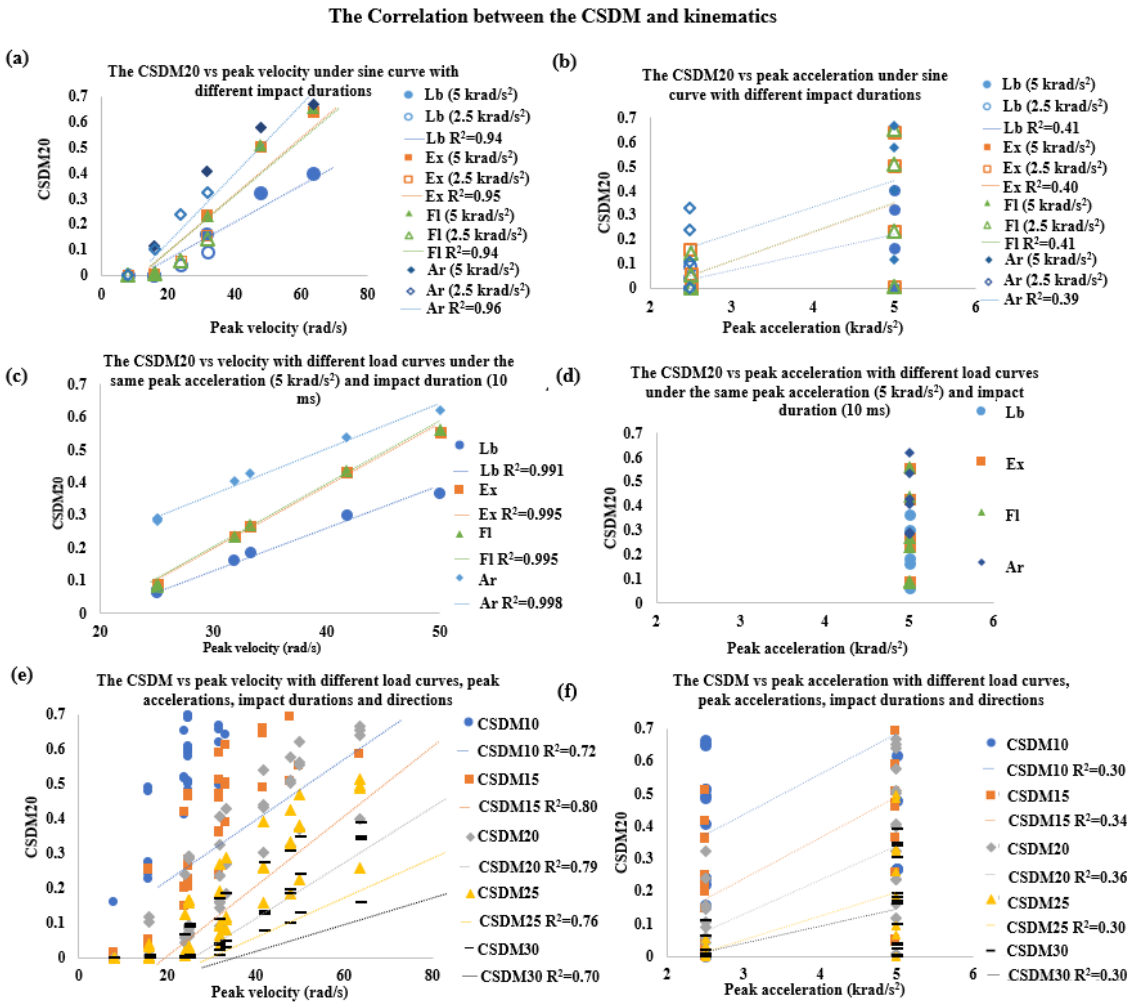


**Figure 2.7 Correlation between the CSDM and rotational velocity. (a) Correlation between CSDM and peak rotational velocity under sine curve with different impact durations; (b) the CSDM20 as a function of peak rotational velocity under different loading curves with the peak acceleration (5 krad/s$^2$) and impact duration (10 ms); (c) correlation between the CSDM20 and peak velocity with different loading curves under the same peaking acceleration (5 krad/s$^2$) and impact duration (10 ms); (d) correlation between the CSDM20 and peak rotational acceleration with different loading curves under the same peaking acceleration (5 krad/s$^2$) and impact duration (10 ms); (e) correlation between the CSDM and peak rotational velocity under all directions and loading curves with different shapes, peak accelerations, impact durations and directions; (f) correlation between the CSDM and peak rotational acceleration under all directions and loading curves with different shapes, peak**

**accelerations, impact durations and directions. Lb: Lateral bending. Ex: Extension. Fl: Flexion. Ar: Axial rotation.**

## 2.4 Discussion

### 2.4.1 CSDM of different brain regions due to rotational impact

The axial rotation produced the highest CSDM within the whole brain. Similar results were found in other CSDM levels (Appendix B). Our finding is consistent with Elkin et al.'s observation, which reported that eccentric impacts (induced axial rotation) produced higher strains compared to jaw impact [48]. Zhang et al. found that lateral-bending impacts produced the highest shear stress levels than frontal impacts [49], while we found that flexion and extension caused higher CSDM values than that of lateral bending. We also found that flexion and extension produced similar strain levels in brain tissue. However, Krave et al. subjected rabbits under rotational loadings and found that flexion induced more brain injury than extension did [102]. The geometrical difference of head structure between human and rabbit may contribute to differences between our and Krave et al's results. Lateral bending produced the lowest strain level, possibly because stiff falx and tentorium prevented the brain from deforming much. As impact directions affected brain response, our results supported developing the brain injury criteria considering direction effects [32].

Kleiven reported that the threshold of the CSDM10 of 50% possibility injury risk for the white matter was 0.47 [25]. In addition, Kleiven reported that over 0.5 MPS appeared in the corpus callosum under axial rotation [103]. Our data showed that the CSDM10 values of the corpus callosum, the basal ganglia and the thalamus which belong to white matter were different under different impact directions. Since brain responses to different brain regions under various directional impacts were different, it is ideal to consider different brain regions when investigating brain injury criteria.

### 2.4.2 The influence of linear acceleration

The tiny influence was imposed by the linear kinematics when it was combined with the rotational kinematics. Based on our result (Table 2.1), the slight change of the CSDM existed when the linear impact was combined with rotational impact being compared to the

rotational impact alone. Most of RMD values which indicate the difference of the strain produced by combination of linear & rotational impacts and pure rotational impacts were around 1. Our result is consistent with findings of other groups. King et al. demonstrated that the rotational acceleration would be the essential cause of brain strain [86]. Kleiven showed that rotational kinematics was important to brain deformation [25]. Interesting, we also found that when forward linear motion was combined with lateral bending, brain strain was slightly lower than that produced by the pure lateral bending. Overall, the influence of linear acceleration on brain strain was small.

### 2.4.3 The role of rotational deceleration

We found that the brain responses to the cases with and without the deceleration were different. The CSDM values of the deceleration were higher than those without deceleration when the impact durations were equal to and larger than 30 ms (Figure 2.5), while the CSDM values of impacts with deceleration was lower than that without deceleration when the deceleration duration was within 20 ms. These results demonstrated the importance of deceleration duration. We also found that axial rotation with deceleration induced the highest CSDM difference compared to that without deceleration (the highest CSDM difference reached to 50%) (Appendix C). Moreover, with the same deceleration loading curves, the axial rotation produced higher CSDM difference than the lateral bending and extension did. Considering rotational deceleration will be critical for developing a more effective rotational-velocity-based the brain injury criteria.

### 2.4.4 The effects of loading-curve shapes

Brain strain varied when loading-curve shapes changed under rotational accelerations with the same peak and duration. Generally, the rectangular curve induced the largest strain distribution, while the triangular curve produced the lowest strain distribution. This is due to the velocity integrated from the rectangular curve was higher than that of the triangular curve. The integrated velocity of rectangular curve was 50 rad/s, higher than that integrated from the triangular curve which was 25 rad/s (Figure 2.6). Hence, higher velocity of the loading curves produced higher strain distributions. The same reason can also be used to explain why the trapezoid curve with the peak acceleration occupying 2/3 of the duration

produced the second largest strain distribution, followed by that with the peak acceleration occupying 1/3 of the duration, and the sine curve. For the four triangular loading curves, with the same integrated rotational velocity of 25 rad/s, CSDM produced by the triangular curve with the acceleration peaking at 2/3 of duration was 0.01 higher than the CSDM from the other three loadings. Moreover, Post et al. used the loading curves which is similar to the sine curve and reported that the loading curve with the acceleration peaking lately and produced higher strain responses [75]. However, we found that based on the same integrated rotational velocity, the curves with the acceleration peaking at 2/3 rather than the end of the duration produced slightly larger strain distribution (Figure 2.6). The differences between two groups could be partially due to the use of different human head models. The correlation between rotational velocity and CSDM

We found there existed strong correlations between the CSDM and rotational velocity but weak correlation between the CSDM and rotational acceleration. Under the curves with the same shape (sine curve) with different peak accelerations and durations with specific directions, the lowest $R^2$ of rotational velocity and the CSDM20 reached to 0.94 (Figure 2.7a), which indicates that under a specific impact direction and a load curve shape, the correlation between the CSDM and the rotational velocity is strong regardless of different impact durations. This correlation remained strong when loading curves with different shapes were considered (Figure 2.7c). Takhounts et al. also reported good correlation between max resultant rotational velocity and CSDM ($R^2$ of 0.91) [32]. When grouping all directions as well as the peak accelerations, durations and load curve shapes, correlations between the CSDM and rotational velocity decreased but still not low with $R^2$ between 0.70 and 0.80 (Figure 2.7e), while $R^2$ of the CSDM and rotational acceleration was within the range of 0.30-0.40 (Figure 2.7f). Knowles et al. reported that there existed the high correlation ($R^2$ of 0.86) between the change of resultant rotational velocity and the CSDM15 with the consideration of different impact locations of helmet [104]. Our data showed that the $R^2$ of rotational velocity and the CSDM15 was 0.80 when impact directions and load curve with different shapes were considered (Figure 2.7c). Gabler et al. stated that brain deformation mainly depended on rotational velocity in short-duration impacts, but it depended more on the rotational acceleration in long-duration impacts [105]. The cases we studied were based on the events of sports-related concussion, for which the durations were

no more than 30 ms. It can be specified that based on our study with impact durations 5 to 20 ms, velocity correlates well to the CSDM. Together with the literature, our study supported the use of rotational velocity instead of acceleration as a predictor of brain injury for impacts with a major positive phase lasting equal to and less than 20 ms.

## 2.5 Conclusions

We systematically investigated how head kinematics -- which included various rotational magnitudes (2.5 and 5 krad/s$^2$), linear plus rotation, various durations (15, 20, 25 and 30 ms), with and without deceleration, various loading-curve shapes -- affected brain strain. We found that axial rotation produced highest strain loading to the whole brain while lateral bending produced lowest strain. Meanwhile, the same lateral bending produced highest strain to the corpus callosum and the thalamus. Flexion and extension produced similar, middle-level strains to the whole brain while they produced highest strains to the basal ganglia. These various effects of impact direction on the whole-brain and deep-brain structures are important for concussion prevention as deep brain structures have been suggested to be concussion relevant. Our data also concurred with the literature that rotation is the main cause of brain strain (over 99%). Furthermore, our data highlighted the importance of rotational deceleration and found that shorter deceleration duration of 10 ms reduced the CSDM20 up to 17% while longer deceleration duration of 30 ms increased the CSDM20 up to 27%. Such finding suggests the potential of optimizing deceleration at a fast speed for future protection gear design. Lastly, our data demonstrated that rotational velocity, rather than rotational acceleration, correlated to brain strain with an average $R^2$ of 0.79 across various impact directions and different shapes of loading curves. When grouping impacts to four direction groups, the correlation between rotational velocity and brain strain reached to an average $R^2$ above 0.94, including various loading-curve shapes.

# Chapter 3

# 3 A systematic study of the helmet protection mechanism

The mechanism of how the helmet protect the brain were analyzed. The energy absorption ratios that helmet parts contributed were evaluated. The correlation between energy absorbed by the helmet, scalp and skull and brain strain distribution result was investigated.

## 3.1 Introduction

Head safety was emphasized as early as in late 19$^{th}$ century due to cranial injuries including brain injuries [106]. Wearing a helmet is an effective way to protect the brain [107]. The number of brain injury-related deaths in American football events was reduced from 150 in 1965-1974 to 25 in 1985-1994 when helmet was used [50]. With the helmet being regulated by committees such as National Operating Committee on Standards for Athletic Equipment (NOCSAE), head injuries reduced from 4.25 per 100,000 to 0.68 per 100,000 [108]. Moreover, Rowson et al. reported that helmet could reduce the occurrence of concussion [51]. Trotta et. al reported that helmet could decrease 65% risk of brain injury from cycling [52]. Motorcycle helmets were also proved to be effective in brain injury protection [109]. Karus et al. demonstrated that a well-designed hockey helmet can decrease 8.3 head injuries per 100 games to 3.8 head injuries per 100 games [54].

Helmets were designed to reduce brain injury risk with the improved structure designs [110]. Viano et al. reported that updated helmet design could reduce brain injury risk [53]. As expected, the performance of the helmet in brain injury risk reduction varies by different helmets [28]. Meanwhile, Rowson et al. reported that a helmet was unable to protect the head completely from all injuries [51]. Hence, helmet structure has been continuously optimized for more effective brain injury protection. For a typical helmet, the outer layer of the helmet is a hard shell [111]. The foam pads were designed as the liner beneath the outer shell with the material that can absorb energy [112, 113]. The facemask, which is at the front of the helmet, prevents athletes from face injury [114]. Although all helmet parts are assumed to play a role in protecting the brain, it is not clear how these components act to reduce brain injury during impacts. Meanwhile to improve helmets, it is necessary to

understand how helmet components contribute to brain injury reduction hence better designs can target critical helmet parts.

The helmet performance was usually evaluated by investigating whether brain injury risk was reduced when using a helmet [115]. Different brain injury criteria have been used to predict brain injury risk. Current brain injury criteria are based on head acceleration because head acceleration was reported to be correlated to brain injury [86]. Hoshizaki et al. demonstrated that the helmet can protect the brain when peak linear acceleration was below 250g [56]. Besides peak acceleration, impact duration was included in test standards of helmets. The Gadd Severity Index (GSI) and the Head Injury Criterion (HIC), which include both acceleration magnitude and impact duration, were used as the standards to test helmets [57, 58, 60]. However, the laboratory tests have some limitations. The dummy head and neck are stiffer than those of real humans [60], which induced higher kinematic responses than they should be. Moreover, the dummy kinematic predictors had limitations to predict brain injury, such as concussion [58]. Compared to dummy kinematic responses, brain tissue strain was demonstrated as an appropriate predictor to brain injury [25, 45, 59, 116]. Using of brain strain to predict brain injury was supported by in vitro studies demonstrating correlations between strain and neuronal damage [62, 117]. Moreover, the brain pressure was used as one of predictors for TBI [118], as it was responsible for the cerebral blood flow [119]. Hence, it is necessary to evaluate the effectiveness of helmet based on brain strain and pressure beyond existing head kinematics.

The objective of this study was to evaluate whether the helmet can reduce brain injury based on brain strain and pressure response. Specifically, we investigated impact energy absorption of different helmet components.

## 3.2 Method

### 3.2.1 Finite element models

The well-defined finite element (FE) model, Global Human Body Model Consortium (GHBMC) head & neck model was used to evaluate the brain responses [96]. There were 297 components, 526,635 elements and 501,961 nodes in the GHBMC head & neck model (Figure 3.1a). The element size was around 3 mm in general. The head part was highlighted

by brain regions including the white matter, grey matter, cerebellum, brain stem and the deep-brain structures such as the corpus callosum, basial ganglia and thalamus. The head bone parts involving the skull, mandible and nose bone were also established. The neck part consisted of the spinal cord, cervical bones, discs and facet joints. A viscoelastic material was used for the white matter, grey matter, cerebellum, corpus callosum, basal ganglia, thalamus, cerebrospinal fluid (CSF) and brain stem [36].More information can be found in Appendix A. The linear plastic material was used in the head bone part including the skull, nose and mandible. The spinal cord and facet joints were created with the viscoelastic material. For other neck bones, the plastic material was used. Both the rubber/foam and the viscoelastic material were used in the disc. The GHBMC head model was validated against the pressure and the brain displacement based on the cadaver tests. The GHBMC neck model was validated in extension and flexion loading at the segmental level [96, 120]. The whole head & neck model was validated in frontal and lateral impact [121].

The open source Riddell Speed Classic helmet FE model (model R41179) [122] was also downloaded from Biocore website [1] and included in this study (Figure 3.1b). There were 57 components, 147,445 elements and 141,015 nodes in the Riddell helmet model. Shell, foam pad, facemask and chinstrap were involved in the helmet model. The outer layer of the helmet, shell, was composed of the shell elements. The elastic material with the young's modulus of 1.565 GPa was used in the shell [122]. The inner layer of the helmet was the foam with the Fu Chang foam material. The facemask, which was established using the beam elements with the elastic material, connected to the helmet outer shell rigidly. The fabric material was used in the chinstrap. The foam material of the helmet was validated against the force and displacement result from shear and compression test [122]. Combined with the Hybrid III dummy model, the Riddell helmet model was validated by the pendulum and linear impact against the contact force and acceleration [122].

The pre-deformation process was adopted to make the inner layer of the Riddell helmet model tightly fitted to the head with the max gap of 4 mm. (Figure 3.1c). Through this process, the head model was used to press the helmet foam pads through left, right and upward directions in sequence. As the pre-deformation process could change mesh

qualities when simulating deformation during wearing a helmet, we checked mesh qualities after pre-deformation and ensured that 99.98% elements had Jacobian above 0.4, with minimum above 0.22. Ls-PrePost version 4.3 was used for the simulation preparation and analysis [100]. Ls-Dyna R901was used to calculate simulations [101]. The timestep of the simulation was within the range of 0.05-0.1 ms.

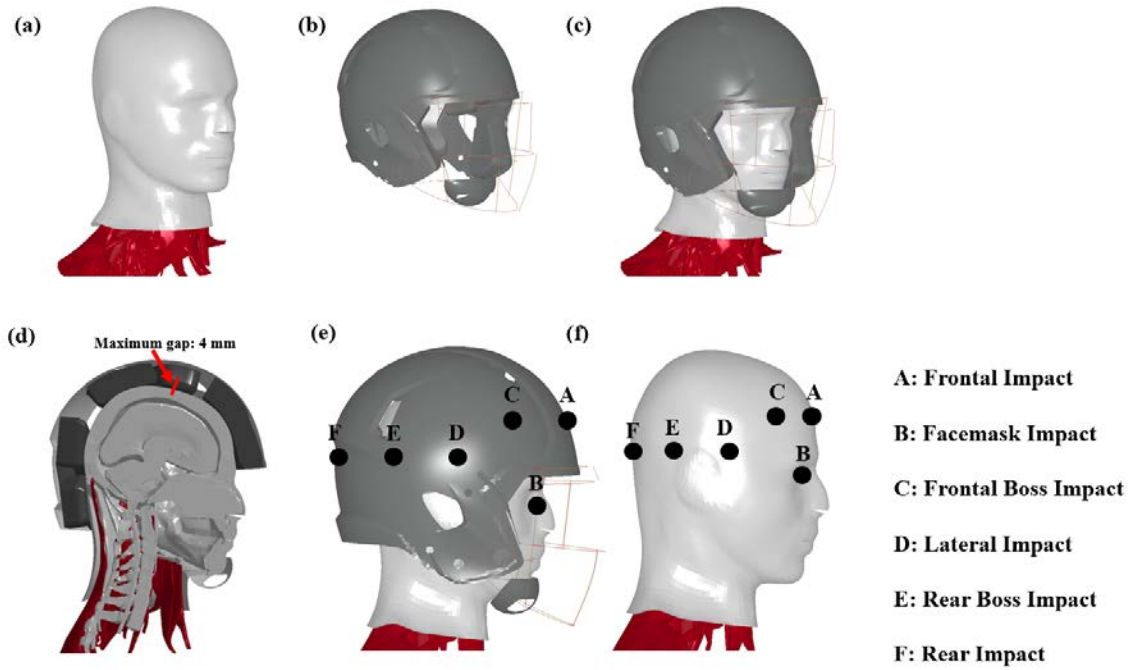


**Figure 3.1 Global Human Body Model Consortium (GHBMC) head & neck model and Riddell helmet model. (a) GHBMC head & neck model; (b) Riddell helmet model; (c) combination of head & neck and helmet model; (d) Impact locations of the head & neck model with helmet; (e) Impact locations of head & neck models without helmet.**

### 3.2.2 Impact conditions

To quantify the effect of the helmet to protect the brain, the impactor (with the length of 121 mm) [1, 123] under the velocity of 6m/s based on the NOCSAE standard [124] was used to impact the frontal site, frontal boss site, lateral site, rear site, rear site and the frontal facemask site of the helmeted head &neck model (Figure 2.1d) and head &neck model without helmet (Figure 2.1e). The total impact duration was 20 ms.

### 3.2.3 Analysis method

#### 3.2.3.1 Brain response

The cumulative strain damage measure (CSDM) with brain strain level of 15%, which means the proportion of brain volume exceeding the peak strain of 15% to the whole brain volume, was used to quantify brain strain distribution [32]. The peak pressure of the head was also included. Under the same impact condition, the CSDM15 results and peak pressure which represents the maximum brain pressure of the brain from helmeted head & neck model and the bare head & neck model were compared to demonstrate the effectiveness of the helmet to protect the brain. The acceleration impulse of head under lateral and rear impact was also demonstrated. CSDM20 results, which means the proportion of brain volume exceeding the peak strain of 20% to the whole brain volume, was attached in Appendix E.

#### 3.2.3.2 Strain energy of helmet

To quantify how helmet protected the brain, the strain energy of the helmet components, scalp and skull which were produced due to deformation was calculated to represent how much energy the specific helmet part absorbed during the impact. This study included the ratio of the specific component's strain energy over the whole energy absorbed during one impact.

## 3.3 Results

### 3.3.1 Response of the head with and without the helmet

#### 3.3.1.1 Brain distribution of the head with and without the helmet

Figure 3.2 included the CSDM15 result of helmeted and bare head under different impacts. The CSDM15 was calculated to describe the strain distribution with and without the helmet. Under the frontal impact to the helmet, the CSDM15 of the brain with the helmet was 0.26, and the CSDM15 increased to 0.32 when the head was not equipped with a helmet (Figure 3.2a). Under the frontal boss impact, the CSDM15 of the head with the helmet was 0.42. The CSDM15 reached to 0.68 when the head didn't wear the helmet (Figure 3.2b). Under lateral impact, the CSDM15 were 0.20 and 0.48 for with, and without

helmet conditions, respectively (Figure 3.2c). Under the rear boss impact, the CSDM15 was 0.26 when the head was equipped with a helmet. When the helmet was removed, the CSDM15 was much higher (0.60) (Figure 3.2d). Rear impact induced the CSDM15 of 0.16 and 0.39 of the brain with and without helmet, respectively (Figure 3.2e). Impact to facemask caused the CSDM15 of 0.46 and 0.62 of brain with and without helmet conditions respectively (Figure 3.2f). High strain was induced by facemask because axial rotation was induced with the moment arm of 119 mm for with-facemask condition, compared to the moment arm of 63 mm for without-facemask condition.

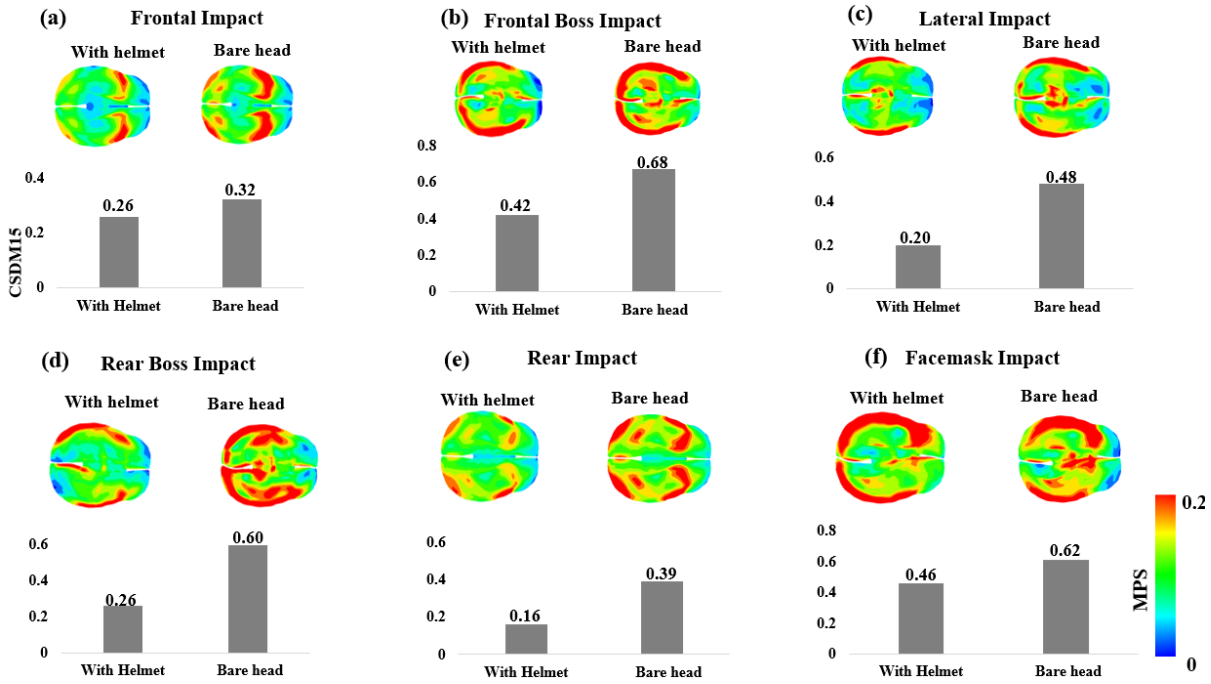


**Figure 3.2 Brain strain distribution of helmeted and bare head under frontal impact (a), frontal boss impact (b), lateral impact (c), rear boss impact (d) rear impact (e) and facemask impact.**

### 3.3.1.2 Pressure of the head with and without helmet

Under the frontal impact, the peak pressure reached to 116 kPa and -69 kPa of the head with the helmet, while it reached to 115 kPa and -93 kPa when the helmet was removed (Figure 3.3a). Under the frontal boss impact, the peak pressure was 94 kPa and -40 kPa when head was equipped with the helmet, while the peak pressured increased to 126 kPa

and -62 kPa when the helmet was removed (Figure 3.3b). Under the lateral impact, the peak pressure was 86 kPa and -90 kPa when the helmet was included (Figure 3.3c). The peak pressure increased to 156 kPa and -137 kPa when the helmet was removed (Figure 3.3c). Under the rear boss impact, peak pressure was 99 kPa and -70 kPa when the head was equipped with the helmet, it increased to 143 kPa and -118 kPa when the helmet was removed (Figure 3.3d). Under the rear impact, the peak pressure was 113 kPa and -70 kPa when the helmet was included (Figure 3.3e). The peak pressure increased to 146 kPa and -117 kPa when the helmet was removed (Figure 3.3e). Under the facemask impact, peak pressure reached to 81 kPa and -128 kPa when the head was equipped with the helmet, while it increased to 109 and -152 kPa when the helmet was removed (Figure 3.3f).

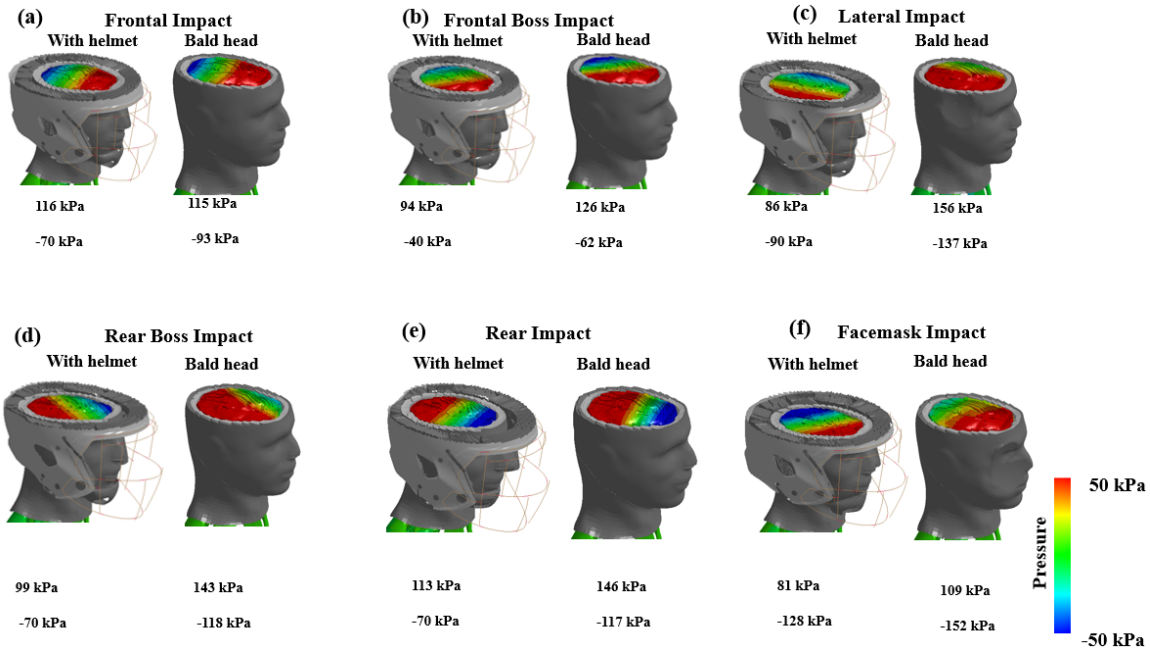


**Figure 3.3 Peak pressure of the head with and without helmet.**

### 3.3.1.3 Acceleration of the head under impact

Head acceleration impulse was generated when head was impacted. Under lateral impact, the acceleration curve peaked at 9.0 ms with peak linear acceleration of 129g (Figure 3.4 a). When helmet was removed, the linear acceleration peaked at 4.5 ms, with peak linear acceleration of 165g (Figure 3.4c). Under rear impact, the acceleration curve peaked at 7.5 ms with peak linear acceleration of 120g (Figure 3.4 b). When helmet was removed,

the linear acceleration peaked at 5 ms, with peak linear acceleration of 181g (Figure 3.4 d).

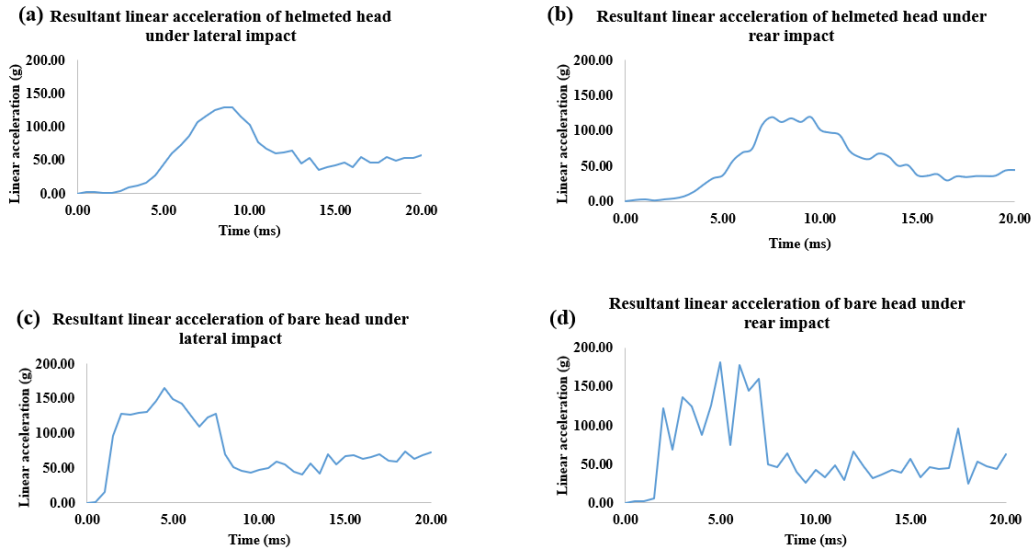


**Figure 3.4 Acceleration impulse of head with and without helmet under lateral and rear impact. Resultant linear acceleration of helmeted head under (a) lateral impact, (b) rear impact; Resultant linear acceleration of bare head under (c) lateral impact, (d) rear impact.**

### 3.3.2 Strain energy absorption of helmet component

During the impacts, the helmet protected the brain by absorbing the energy. Figure 4 and Table 1 showed the percentage of the energy that various helmet parts absorbed. During the frontal impact, shell of the helmet absorbed 59.6 % of energy (Figure 3.5a and Table 3.1). The frontal foam which was beneath the shell and the location that the impactor hit the helmet absorbed 28.6% of the energy (Figure 3.5b and Table 3.1). The scalp and skull absorbed 0.9% and 0.9% energy, respectively (Figure 3.5c, 3.5d and Table 3.1). Other helmet components absorbed the remaining 10.0% energy. Under the frontal boss impact, the shell absorbed 53.9% of the total energy (Figure 3.5e and Table 3.1). The foams which were close to the impact location absorbed 32.3% of the total energy (Figure 3.5f and Table 3.1). The scalp absorbed 4.3% energy (Figure 3.5g and Table 3.1). The skull absorbed 0.3% energy (Figure 3.5h and Table 3.1). Other helmet components absorbed 9.2% of the energy.

During the lateral impact, shell absorbed 44.3% of the total energy (Figure 3.5i and Table 3.1). The foam components which were located near the impact location absorbed 14.0%, 8.0% and 22.1% of the total energy (Figure 3.5j and Table 3.1). The scalp absorbed 4.5% of the energy (Figure 3.5k and Table 3.1). Other helmet components absorbed 6.6% energy (Table 3.1). Under the rear boss impact, shell absorbed 49.4% of the energy (Figure 3.5m and Table 3.1). The foams which were at the rear site of the helmet absorbed 4.2% and 32.5% of the total energy (Figure 3.5n and). 3.6% of the energy was absorbed by the scalp (Figure 3.5o and Table 3.1). The skull absorbed 0.4% of the energy (Figure 3.5p and Table 3.1). Other helmet components absorbed 9.9% of the total energy (Table 3.1). Under the rear impact, shell absorbed 37.0% of the energy (Figure 3.5q and Table 3.1). The foams which were at the rear site of the helmet absorbed 16.7%, 3.1% and 24.3% of the total energy (Figure 3.5r and Table 3.1). The scalp absorbed 3.5% energy (Figure 3.5s and Table 3.1). The skull absorbed 0.2% of the energy (Figure 3.5t and Table 3.1). Other helmet components absorbed 15.2% of the total energy (Table 3.1). Under the impact to facemask, shell absorbed 47.6% of the energy (Figure 3.5u and Table 3.1). The foams which were at the rear site of the helmet absorbed 13.7%, 3.4% and 12.1% of the total energy (Figure 3.5v and Table 3.1). The scalp absorbed 9.5% of the energy (Figure 3.5w and Table 3.1). 1.0% energy was transferred to the skull (Table 3.1). Other helmet parts absorbed 12.7% energy (Figure 3.5x and Table 3.1).

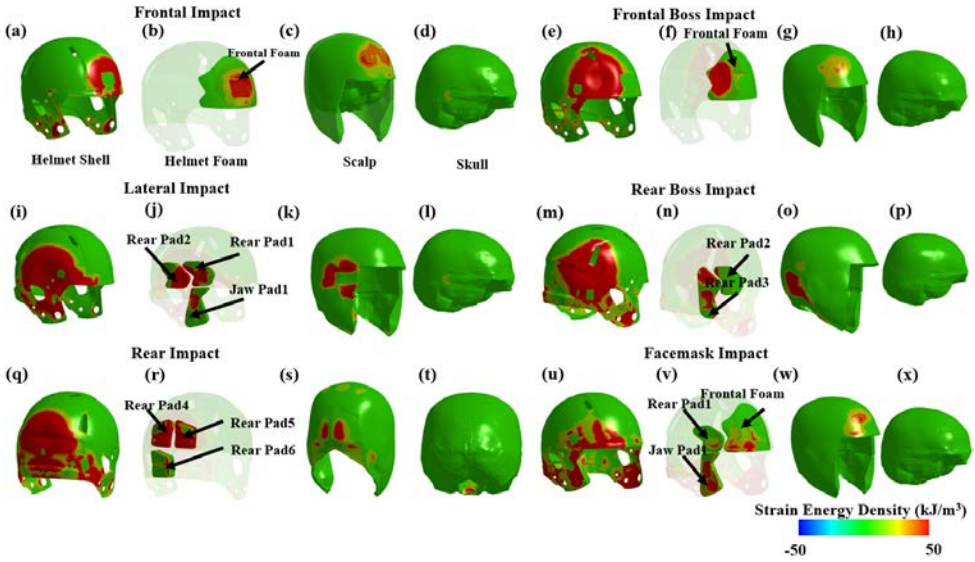


**Figure 3.5 Energy absorption of helmeted components.**

**Table 3.1 Energy absorption percentage of helmet components.**

| Impact Location | Foam Components | Percentage |
|---|---|---|
| Frontal Impact | Shell | 59.6% |
| | Frontal Foam | 28.6% |
| | Skull | 0.9% |
| | Scalp | 0.9% |
| | Other | 10.0% |
| Total Energy | 44.0 J | |
| Frontal Boss Impact | Shell | 53.9% |
| | Frontal Foam | 32.3% |
| | Skull | 0.3% |
| | Scalp | 4.3% |
| | Other | 9.2% |
| Total Energy | 126.6 J | |
| Lateral Impact | Shell | 44.3% |
| | Rear Pad1 | 14.0% |
| | Jaw Pad1 | 8.0% |
| | Rear Pad2 | 22.1% |
| | Skull | 0.5% |
| | Scalp | 4.5% |
| | Other | 6.6% |
| Total Energy | 105.8 J | |
| Rear Boss Impact | Shell | 49.4% |
| | Rear Pad2 | 4.2% |
| | Rear Pad3 | 32.5% |
| | Skull | 0.4% |
| | Scalp | 3.6% |
| | Other | 9.9% |
| Total Energy | 117.5 J | |
| Rear Impact | Shell | 37.0% |
| | Rear Pad3 | 16.7% |
| | Rear pad4 | 3.1% |
| | Rear Pad5 | 24.3% |
| | Skull | 0.2% |
| | Scalp | 3.5% |
| | Other | 15.2% |
| Total Energy | 110.4 J | |
| Facemask Impact | Shell | 47.6% |
| | Frontal Foam | 13.7% |
| | Rear Pad1 | 3.4% |
| | Jaw Pad1 | 12.1% |
| | Skull | 1.0% |
| | Scalp | 9.5% |
| | Other | 12.7% |
| Total Energy | 56.3 J | |

### 3.3.3 Correlation between brain strain distribution and energy

The amount of energy the helmet absorbed was different as the impact location varied (Figure 3.6). The helmet, scalp and skull absorbed the strain energy of 44.0 J under frontal impact, 126.6 J under the frontal boss impact, 105.8 J under lateral impact, 117.5 J under rear boss impact, 110.4 J under the rear impact and 56.3 J under the rear impact (Table 3.1). The $R^2$ of the CSDM15 and absorbed strain energy was 0.31 (Figure 3.6).

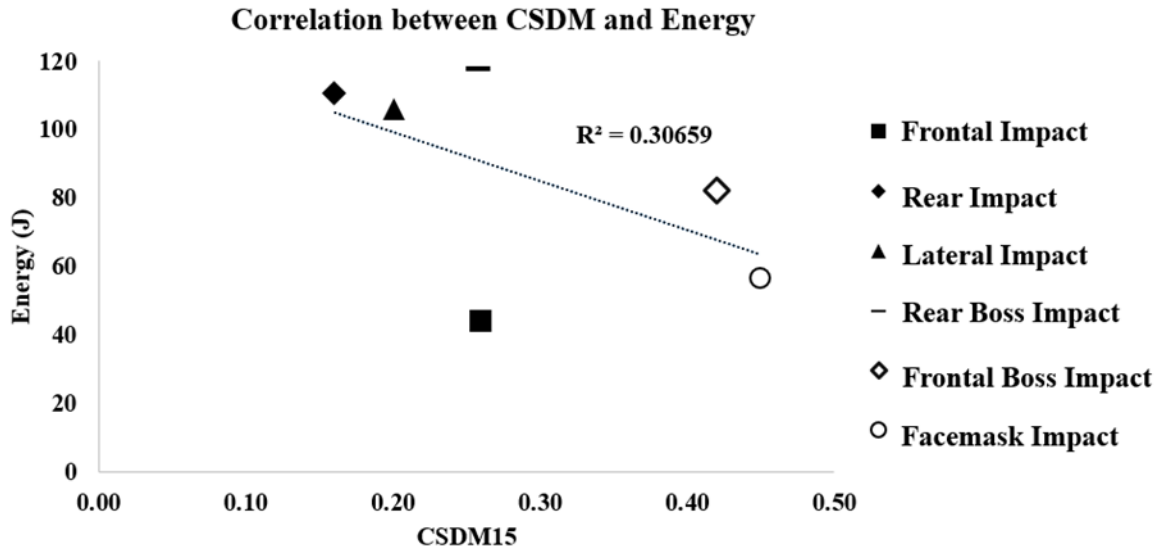


**Figure 3.6 Correlation between CSDM15 and energy absorbed by helmet.**

## 3.4 Discussion

### 3.4.1 The response of head under impat

#### 3.4.1.1 The effectiveness of helmet to protect the brain

While helmets being demonstrated to reduce head kinematics during traumatic events [125], we characterized how the helmet reduced brain strain. We found that the helmet reduced brain strain distribution measure the CSDM15 by 18.8% during frontal impact, 37.3% during frontal boss impact, 56.7% during lateral impact, 58.9% during rear impact, and 24.3% during impact to the facemask. Newman reported that the helmet could decrease the peak linear and rotational acceleration of head by 68.5% and 41.6% respectively under frontal impact [125]. We also found that helmet decreased the peak pressure of the brain.

Lewis et al. demonstrated that helmet can reduce head peak linear acceleration by at least 30% [126]. Cripton et al. reported that bicycle helmets could reduce head peak linear acceleration by 76.3% in the drop test with the drop height of 2 m [127]. With the understanding that the brain response especially strain response causing injury, our research served as a pioneering study in promoting the understanding how a helmet protects the brain.

#### 3.4.1.2 Acceleration impulse of head under impacts

The acceleration impulse was different for bare-head and helmeted impacts. Under lateral impact, acceleration impulse of bear head impact peaked earlier and demonstrated higher peak acceleration (Figure 3.4 a and c). The acceleration impulse of head with helmet was smooth around peak occasion while there were several fluctuations around peak occasion for helmeted impact (Figure 3.4 b and d).

### 3.4.2 Energy absorption by helmet components

We quantified how various components of the helmet contributed to reducing impact energy. Interestingly, we found that the outer shell absorbed most portion of energy compared to other parts including soft foam pads that were designed to absorb impact energy. Among all impacts in six directions, the shell absorbed an average 49.5% (standard deviation of 6.5%) of energy and the foam pads absorbed an average 17.3% (standard deviation of 11.5%) of energy. It should be noticed that the shell and foam directly under impact absorbed energy (Figure 3.5 and Table 3.1), while some remote shells also absorbed energy (Figure 3.5) because the helmet was constructed as a structure. The role of the scalp in energy absorption during impact can't be ignored [52]. Our result indicated that the scalp absorbed an average 5.0% of energy (standard deviation of 2.3%). The skull absorbed the lowest energy with average ratio of 0.6% (standard deviation of 0.3%).

### 3.4.3 Correlation between the CSDM and energy

The energy absorbed by the helmet varied as impact location changed because of the anatomy of the geometry of head & neck. The highest energy was absorbed by the helmet, scalp and skull under rear boss impact, while the lowest energy was absorbed under the

frontal impact. However, it should be noticed that how much the helmet absorbed energy was not correlated to the CSDM15 (Figure 3.5), as brain strain distribution was affected by not only impact severity, but also impact location and angle [48, 128]. Our research highlights the importance of protecting the brain under various directions.

## 3.5 Conclusion

By absorbing impact energy, the helmet largely reduced brain strain distribution and peak pressure. The contribution of helmet parts to energy absorption was different, with the helmet shell absorbing around half of the energy, followed by the foams which were close to the impact locations. To the best our knowledge, this is the first study that systematically quantified how different helmet components contributed to energy absorption. The acceleration pulse was different as the inclusion of helmet under lateral and rear impact. We highlighted the importance of optimizing both the hard shell and foam pad to better reduce brain strains. Meanwhile, we highlighted the importance of looking into brain response like strain as impact energy absorption under various directions of impacts didn’t correlate with brain strain distribution measure.

# Chapter 4

# 4 The role of facemask in brain strain

The influence of facemask based on brain strain distribution was evaluated. The correlation between dimension change difference (before and after impact) induced by facemask and brain strain difference caused by facemask was also investigated.

## 4.1 Introduction

Traumatic brain injury (TBI) remains a significant health concern accounting for approximately one-third of injury related deaths in the United States as stated by the CDC. In the US alone, there are approximately 2.8 million patients who suffer from sports-related TBI including concussion [129]. Mild TBIs, more commonly associated with concussions can induce chronic symptoms such as memory loss, cognitive deficits, and balance disturbances. Hence, improving the methods to protect the brain from concussions is of upmost importance for the long-term health benefits of the modern athlete and casual sports participant [5, 6].

The use of a helmet is regarded as an effective method to decrease the likelihood of brain injury [51, 108]. The number of brain injury-related deaths in American football events was reduced from 150 in 1965-1974 to 25 in 1985-1994 with the implementation of the modern helmet [50]. The effectiveness of helmets has not been reported in only contacts sports with Trotta et. al reporting that the use of bicycle helmets during cycling decreased the risk of brain injury by 65% [52].

Currently the only helmet evaluation standards are based on the kinematic responses of a head and neck dummy [124]. While the effectiveness of those standards in reducing the brain injury is outside the scope of this paper, the inclusion of all components of a helmet to determine helmet safety rating is looked at. Within one helmet, there is a combination of different components and materials with the goal of reducing the energy being transferred to the head. The outer component of a typical helmet known as the shell, is used to resist the initial blunt impact directly [111]. Beneath the outermost layer typically lies a combination of different density foams with the goal to absorb additional impact energy

and dissipate linear motion [112, 113]. To constrain the helmet to the head, a fabric chinstrap, sitting below the chin or directly attached to the chin, is used. To prevent facial injury ,including lacerations, the facemask sits on the front of the helmet and is typically constructed of latticed steel bars. [114]. The helmet and facemask can reduce the chances of facial injuries in the ice hockey [130]. Reynen and Clancy reported that facemask may increase the possibilities to get the neck injured because the axial loading was increased to the flexed cervical spine, which may induce burst fracture [131].

The facemask is one component which is currently excluded when evaluating helmet performance standards [65]. The facemask has been evaluated separately by applying force until deformation. One question that this study looks to answer is what significance the facemasks inclusion in helmeted impact testing has to brain strain, which is currently an unknown.

Our hypothesis is that the inclusion of the facemask in helmet testing would affect head kinematic response. Based on pneumatic impactor tests, Rowson et al. found that the influence of the facemask to the peak head acceleration varied by both impact locations and helmet types [65]. Rush et al. reported that facemask increased head kinematics in 62% of the drop tests cases [64]. Breedlove et al. reported that the facemask increased peak head acceleration up to 36% [63]. With the optimized facemask design, Johnson et al. reported that maximum tensile pressure and maximum shear strain of the brain could be decreased by 7.5% and 39.5% respectively [132].

The head kinematic variables from laboratory experiments had the limitations to predict the brain injury [58, 60]. Although head linear kinematics were measured to evaluate brain injury [133], the rotational kinematics were closely correlated to concussion [86, 134, 135]. Moreover, both linear and rotational kinematics were measured based on the dummy head motion, not the brain motion [60]. Compared to the head kinematics, brain strain is regarded as the main reason to induce brain injury [58, 59]. Moreover, the brain pressure was also used to represent TBI [118], as it was responsible for the cerebral blood flow [119]. Hence, it is necessary to know the effect of facemask based on brain strain and pressure, which we investigated in this study.

## 4.2 Methods

### 4.2.1 Finite element (FE) models

This study elected to use the Global Human Body Model Consortium (GHBMC) head & neck model to evaluate the brain responses [96], due to its extensive validation process and anatomical accuracy. The GHBMC head and neck model contained 297 components, 526,635 elements and 501,961 nodes (Figure 4.1a). The element size was around 3 mm in general. The head is highlighted by important brain and skull components including the white matter, grey matter, cerebellum, brain stem and the deep-brain areas such as the corpus callosum, basial ganglia and the thalamus. The skull involves important facial structures such as the mandible, orbital and nasal bones. The neck contains the spinal cord, cervical bones, discs and the facet joints. A viscoelastic material was used in the white matter, grey matter, cerebellum, corpus callosum, basal ganglia, thalamus, cerebrospinal fluid (CSF) and the brain stem [36]. A linear plastic material was used for bone in the skull. More information can be addressed in Appendix A. The spinal cord and facet joints were created with a viscoelastic material. For the remaining neck bones, a plastic material was used. Both the rubber/foam and the viscoelastic material were used in the disc. The model was validated against intracranial pressures and brain displacements [97-99]. The GHBMC neck model was validated in extension and flexion loading at the segmental level [96, 120]. The whole head & neck model was validated in frontal and lateral impact [121].

The helmet model used for this study was Riddell Speed Classic football helmet FE model (model R41179) [122] which was downloaded from Biocore website [1] (Figure 4.1b). A total of 57 components, 147,445 elements and 141,015 nodes exist in the in the Riddell helmet. The helmet model includes standard components; shell, foam pads, facemask and chinstrap, to accurately represent real world geometries. The outer layer of the helmet, the plastic shell, was composed of the shell-type elements, with an elastic material with a young’s modulus of 1.565 GPa. The inner layer of the helmet was foam with the Fu Chang foam material. The foam material of the helmet was validated against the force and displacement result from shear and compression tests. The facemask, which was generated as beam elements with elastic material properties, connected to the helmet outer shell rigidly. The chinstrap was constructed using a fabric-like material. The foam material of

the helmet was validated against the force and displacement result from shear and compression test [122]. Being combined with the Hybrid III dummy model, the Riddell helmet model was validated by the pendulum and linear impact against the contact force and acceleration [122]. Ls-PrePost version 4.3 was used for the simulation preparation and analysis [100]. Ls-Dyna R901was used to calculate simulations [101]. The timestep of the simulation was within the range of 0.05-0.1 ms.

The validated human head model and helmet model were integrated using the validated approach in dummy model validation (Figure 4.1c). Using a preconditioning process, the inner layer of the Riddell helmet model was tightly fitted to the head with maximum gap of 4 mm (Figure 4.1d). Through this process, the head model was used to press the helmet foam pads through left, right and upward directions in sequence.

### 4.2.2 Impact matrix design

Based on the NOCSAE standard, an impactor (with the length of 121 mm) [1, 123] under a velocity of 6 m/s was used in this study [124]. The helmet-to-head friction coefficient was 0.5 [122]. Two categories of test (helmet with facemask and helmet without facemask) were examined. For the helmet with facemask scenario, the impactor was targeted to hit the frontal, lateral, vertical, rear, frontal boss and rear boss sites of the helmet and frontal site to facemask (Figure 4.1e). In comparison, the impactor was also used to hit the same locations of the helmet without the facemask (Figure 4.1f). The total impact duration was 20 ms.

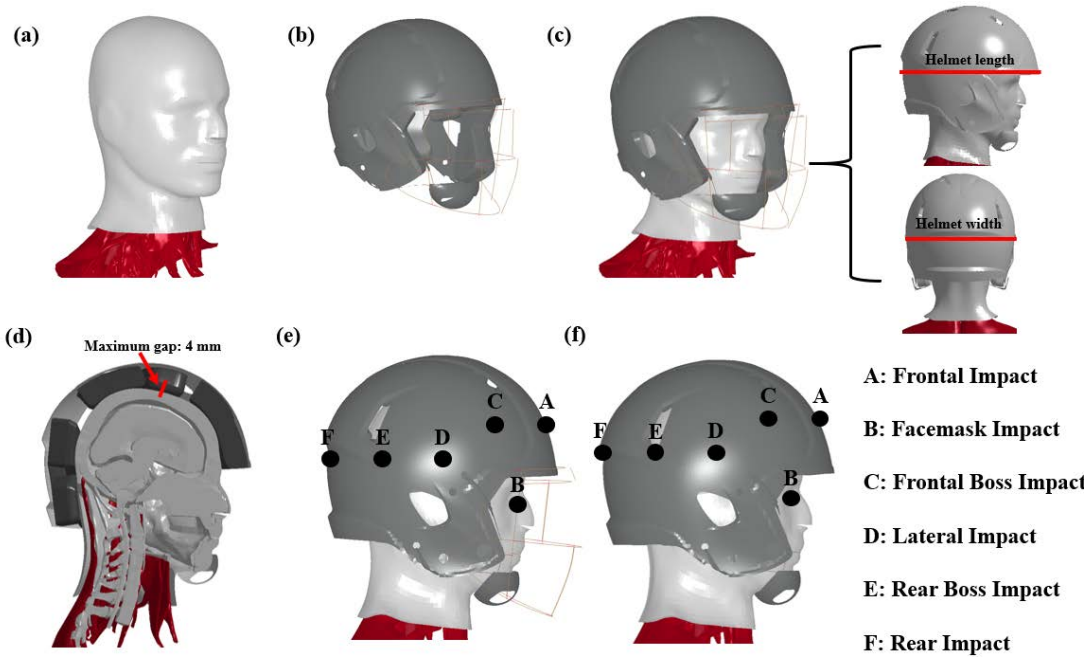


**Figure 4.1 Impact location of the helmet with and without the facemask. (a) Global Human Body Model Consortium (GHBMC) head & neck mode; (b) Riddell Speed Classic football helmet FE model; (c) Combination of head & neck model and helmet model; (d) Maximum gap between head & neck model and helmet model; (e) Impact location of the helmet with facemask; (f) Impact location of the helmet without the facemask.**

### 4.2.3 Analysis method

The cumulative strain damage measure (CSDM) with 15% of brain strain level, which means the proportion of brain volume exceeding the peak strain of 15% to the whole brain volume, was used to quantify brain strain distribution [32]. Under the same impact condition, the CSDM15 results and peak intracranial pressure from the helmet-with-facemask and the helmet-without-facemask were compared to investigate how the facemask affected brain strain and pressure responses. CSDM20 results, which means the proportion of brain volume exceeding the peak strain of 20% to the whole brain volume, was attached in Appendix E. The length and width of the helmet before and after the impact were also explored to quantify how adding a facemask influenced the helmet in protection of the brain. Moreover, the aspect ratio of length and width (Eq.4.1) was calculated based

on the absolute dimension change difference between helmet with and without facemask (Eq 4.2). The length and width aspect ratio was investigated under frontal impact, frontal boss impact, lateral impact, rear boss impact and rear impact, while the length and width aspect ratio of facemask impact was excluded because the face was directly impacted when facemask was removed. The acceleration impulse of head under lateral and rear impact was also demonstrated.

$$Acepct\ ratio.L.W = Absolute\left(\frac{Difference.L}{Difference.W}\right) \quad \textbf{Eq 4.1}$$

Where Acepct ratio.L.W was aspect ratio of helmet length and width difference induced by facemask. Difference.L was absolute length of helmet length. Difference.W was absolute length of helmet width.

$$Difference.D = absolute(Difference.D.WO.F - Difference.D.W.F) \quad \textbf{Eq 4.2}$$

Where Difference.D was absolute dimension difference (before and after impact) induced by facemask. Difference.D.WO.F was dimension change of helmet without facemask. Difference.D.W.F was dimension change of helmet with facemask.

## 4.3 Results

### 4.3.1 Response of the helmeted head with and without the facemask

#### 4.3.1.1 Brain distribution response of the helmeted head with and without the facemask

The CSDM15 results of the helmeted head with and without facemask are listed in Figure 4.2. Under the frontal impact, the CSDM15 of the helmeted head with the facemask was 0.26, when facemask was removed, the CSDM15 increased to 0.28 (Figure 4.2a). Under the frontal boss impact, the CSDM15 results of the helmeted head with facemask (0.42) and without facemask (0.43) were similar (Figure 4.2b). Lateral impact induced the CSDM15 of 0.20 when the helmet was equipped with the facemask, the CSDM15 was increased to 0.23 when the facemask was removed (Figure 4.2c). Under the rear boss impact, the CSDM15 of the helmeted head with the facemask was 0.26 (Figure 4.2d). The

CSDM15 reduced to 0.24 when the facemask was removed (Figure 4.2d). Under the rear impact, the CSDM15 of the helmeted head with facemask was 0.16, while it increased to 0.22 when facemask was removed (Figure 4.2e). Under the direct facemask impact, the CSDM15 of the helmeted head was 0.46, while it decreases to 0.17 when the facemask was removed (Figure 4.2f). Facemask impact induced high strain because axial rotation was induced with the moment arm of 119 mm compared to the moment arm of 69 mm for bare head condition.

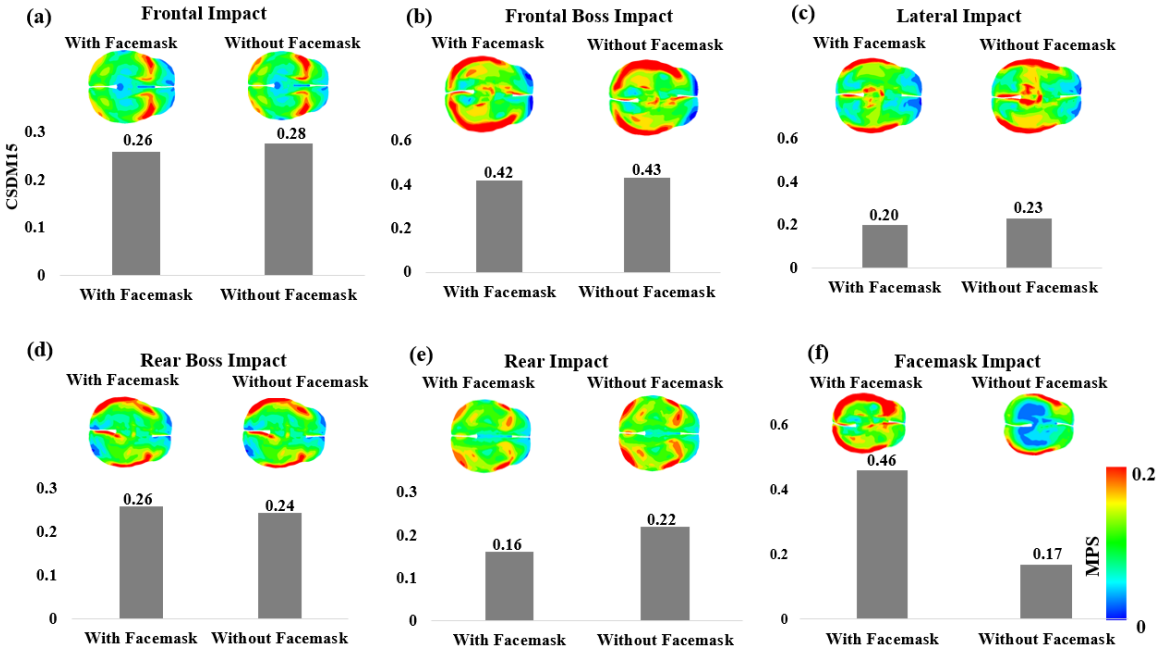


**Figure 4.2 Brain distribution of the helmeted head with and without facemask. Brain distribution of the helmeted head with and without facemask (a) under frontal impact; (b) under frontal boss impact; (c) under lateral impact; (d) under rear boss impact; and (e) under rear impact.**

### 4.3.1.2 Brain pressure response of the helmeted head with and without the facemask

Under the frontal impact, the peak pressure results of coup and contre-coup reached to 116 kPa and -69 kPa, respectively, with the facemask head model, while it reached to 104 kPa and -69 kPa when the facemask was removed (Figure 4.3a). Under the frontal boss impact, the peak pressure was 94 kPa and -40 kPa when head was equipped with the helmet and

facemask combination, while the peak pressured decreased to 84 kPa and -40 kPa when helmet was removed (Figure 4.3b). Under the lateral impact, the peak pressure was 86 kPa and -90 kPa when the facemask was included (Figure 4.3c). The peak pressure changed to 83 kPa and -94 kPa when helmet was removed (Figure 4.3c). Under the rear boss impact, peak pressure was 99 kPa and -70 kPa when the head was equipped with helmet, it remained similar as 100 kPa and -70 kPa when helmet was removed (Figure 4.3d). Under the rear impact, the peak pressure was 113 kPa and -70 kPa when helmet was included (Figure 4.3e). The peak pressure reduced to 101 kPa and -61 kPa when helmet was removed (Figure 4.3e). Under the facemask impact, peak pressure reached to 81 kPa and -128kPa when head was equipped with helmet, while it decreased to 75 and -77 kPa when helmet was removed (Figure 4.3f).

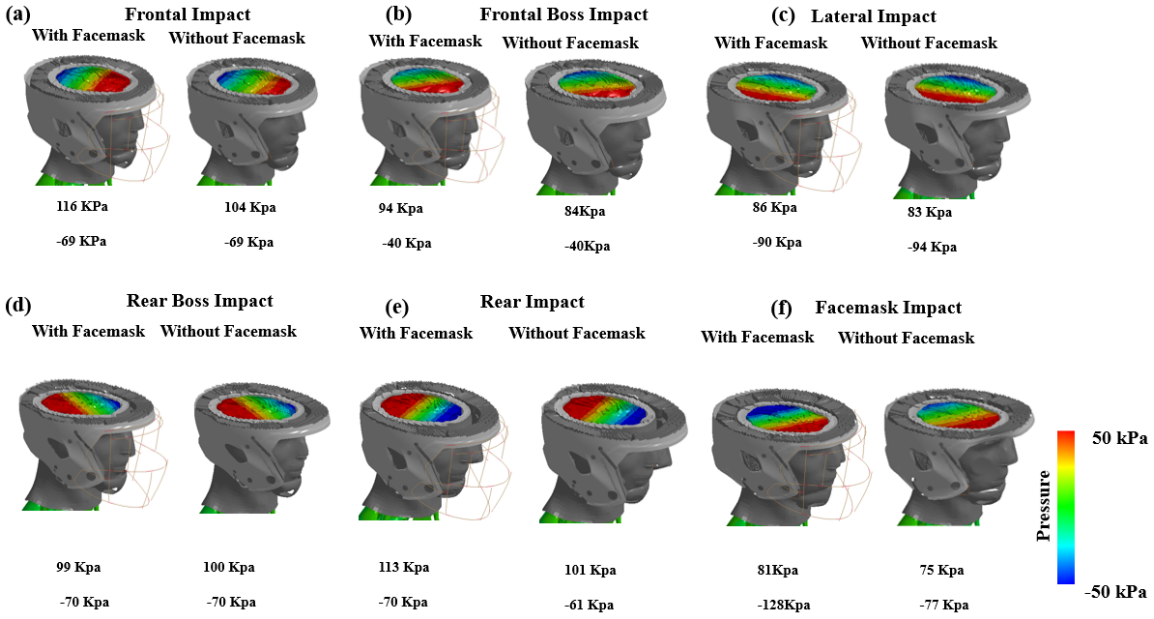


**Figure 4.3 Peak pressure of the helmeted head with and without facemask. (a)Pressure response of frontal impact; (b) Pressure response of frontal boss impact; (c) Pressure response of lateral impact; (d) Pressure response of rear boss impact; (e) Pressure response of rear impact; (f) Pressure response of facemask impact.**

#### 4.3.1.3 Acceleration of head under impact

Head acceleration impulse was generated when head was impacted. Under lateral impact, the acceleration curve peaked at 9.0 ms with peak linear acceleration of 129g (Figure 4.4 a). When facemask was removed, the linear acceleration peaked at 8 ms, with peak linear acceleration of 132 g (Figure 4.4c). Under rear impact, the acceleration curve peaked at 7.5 ms with peak linear acceleration of 120g (Figure 4.4b). When facemask was removed, the linear acceleration peaked at 8.5 ms, with peak linear acceleration of 125g (Figure 4.4d).

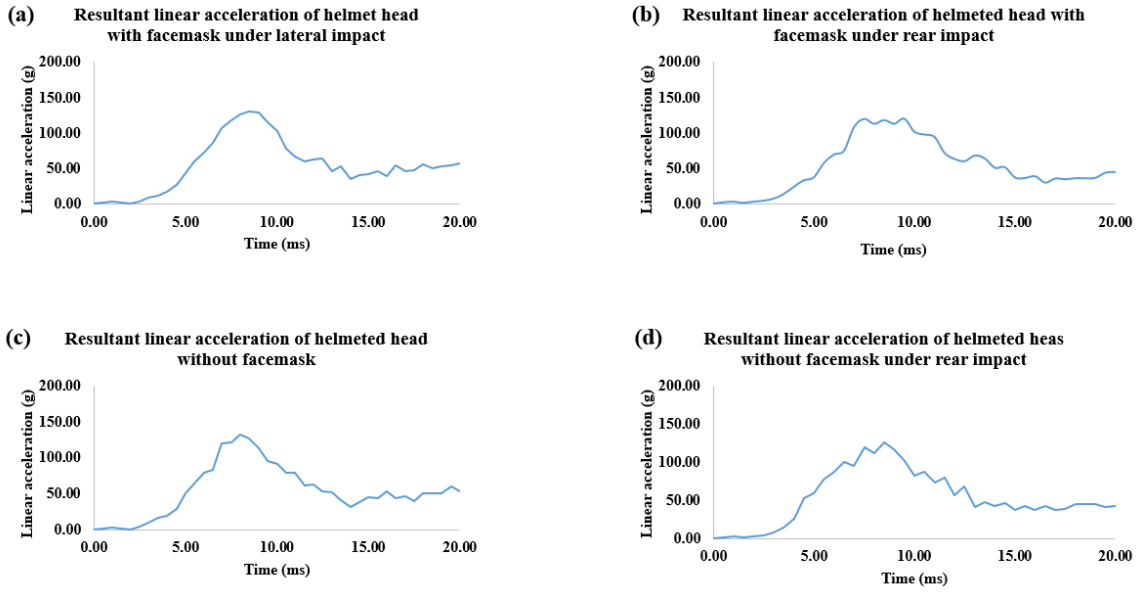


**Figure 4.4 Acceleration impulse of helmeted head with and without facemask under lateral and rear impact. Resultant linear acceleration of helmeted head with facemask under (a) lateral impact, (b) rear impact; Resultant linear acceleration of helmeted head without facemask under (c) lateral impact, (d) rear impact.**

### 4.3.2 Helmet dimension change before and after the impact

The length and width change of the helmet before and after the impact are listed in Table 4.1. Under the frontal impact, the length of the helmet with the facemask increased by 0.3 mm and the width reduced by 1.3 mm after the impact. When the facemask was removed, the length was decreased by 11.4 mm, while the width increased 5.7 mm. The aspect ratio was 1.7 under frontal impact. Under the frontal boss impact, when the helmet was with the

facemask, the length decreased 1.2 mm, while the width increased by 2.1 mm after the impact. When the facemask was removed, the length decreased 0.3 mm after the impact and width decreased by 1.0 mm after the impact. The aspect ratio was 0.3. Under the lateral impact, the length of the helmet with the facemask increased 0.3 mm and the width reduced by 4 mm after the impact. When the facemask was removed, the length was increased 8.9 mm, the width reduced 11.8 mm after impact. The aspect ratio was 1.1. Under the rear boss impact, the length of the helmet with the facemask increased 2.1 while the width reduced 0.2 mm after the impact. When the facemask was removed, the length was increased 5.6 mm and the width reduced by 3.7 mm. The aspect ratio was 1.0. Under the rear impact, the length of the helmet with the facemask reduced 8.3 mm after the impact, while the width increased 2 mm. When the facemask was removed, the length was reduced 3.3 mm, while the width increased 1 mm. The aspect ratio was 5. Under the impact to the facemask, when the helmet was with facemask, the length increased 4.5 mm after the impact and the width reduced by 2.6 mm after the impact. When facemask was removed, the length increased 4.9 mm while the width reduced 2.5 mm after the impact.

**Table 4.1 Helmet dimension change before and after the impact.**

| Impact Location | | **With** Facemask | | | **Without** Facemask | | | |
|---|---|---|---|---|---|---|---|---|
| | Dimension change | Before impact | After impact | Dimension change | Before Impact | After Impact | Dimension change | Aspect ratio |
| Frontal Impact | Length<br>Width | 274.1<br>239.2 | 274.4<br>237.7 | 0.3<br>-1.3 | 274.1<br>239.2 | 262.7<br>244.9 | -11.4<br>5.7 | 1.7 |
| Frontal Boss | Length<br>Width | 274.1<br>239.2 | 272.9<br>241.3 | -1.2<br>2.1 | 274.1<br>239.2 | 273.8<br>238.2 | -0.3<br>-1.0 | 0.3 |
| Lateral Impact | Length<br>Width | 274.1<br>239.2 | 274.4<br>235.2 | 0.3<br>-4.0 | 274.1<br>239.2 | 283.0<br>227.4 | 8.9<br>-11.8 | 1.1 |
| Rear Boss | Length<br>Width | 274.1<br>239.2 | 276.2<br>239.0 | 2.1<br>-0.2 | 274.1<br>239.2 | 279.7<br>235.5 | 5.6<br>-3.7 | 1.0 |
| Rear Impact | Length<br>Width | 274.1<br>239.2 | 265.8<br>241.2 | -8.3<br>2.0 | 274.1<br>239.2 | 270.8<br>240.2 | -3.3<br>1.0 | 5.0 |
| Facemask Impact | Length<br>Width | 274.1<br>239.2 | 278.6<br>236.6 | 4.5<br>-2.6 | 274.1<br>239.2 | 279.0<br>236.7 | 4.9<br>-2.5 | |

## 4.4 Discussion

### 4.4.1 Brain response difference induced by facemask

What this study helped determine was that the influence of the facemask on brain response was dependent on the impact locations. The removal of the facemask induced higher strain distribution under frontal impact, frontal boss impact, lateral impact, and rear impact (Figure 4.2a, 4.2b, 4.2c, and 4.2e). The removal of the facemask decreased brain strain distribution under rear boss impact and facemask impact (Figure 4.2d and 4.2f). Although our CSDM20 (Appendix E) of helmeted head with facemask was higher than that of helmeted head without facemask under frontal impact, the removal of the facemask induced higher strain distribution under frontal impact in general because CSDM15 counted the proportion of brain volume which exceeded wider strain level (15%, rather than 20%) to the whole brain volume. Rowson et al. demonstrated that with the impact velocity of 6m/s, facemask decreased peak rotational acceleration under frontal and lateral impact, while it increased the peak rotational acceleration under rear boss impact [65]. Our result indicated that facemask reduced brain strain distribution under frontal and lateral impact, but it increased the strain distribution under rear boss impact. Breedlove et al.

reported that the facemask increased the peak acceleration under frontal, lateral and rear impact [63]. Since rotational acceleration, rather than linear acceleration, was regarded as the primary cause when inducing brain strain, the facemask may reduce the possibility of a brain injury under frontal and lateral impact. Our result also indicated that brain strain distribution was increased by the inclusion of the facemask when impact was imposed directly to the facemask (Figure 4.2f) because more axial loading was added to the head. On the other hand, since the primary function of the facemask is to protect from facial and scalp injuries [131], the optimization, rather than the removal of the facemask is needed to decrease brain injury [132].

Moreover, we demonstrated that facemask increased the peak intracranial pressure under frontal impact, frontal boss impact, and rear impact and facemask impact (Figure 4.3a, 4.3b, 4.3e and 4.3f). The linear acceleration was reported to be closely correlated to brain pressure [25, 86]. Rowson et al. reported facemask decreased the peak liner acceleration under frontal and lateral impact, while peak linear acceleration was increased under rear boss impact [65]. Our result indicated that facemask reduced both peak coup and contrecoup pressure under frontal impact, but only increased peak coup pressure under lateral impact (Figure 4.3a and 4.3c). Breedlove et al. demonstrated that facemask increased peak acceleration under frontal, frontal boss, lateral and rear impact with the drop velocity of 5.47m/s, while it was not increased by rear boss impact [63]. Our results indicated that the facemask equipped helmet increased peak acceleration under frontal impact, frontal boss impact, and rear impact. Meanwhile the helmeted head, with and without facemask, had the similar peak pressure results under rear boss impacts.

### 4.4.2 Acceleration impulse of head under impacts

The removal of facemask produced more fluctuations of impulse. Under lateral impact, the helmeted head with facemask generated smooth impulse, while different fluctuations existed around the peak accelerations of the impulse from helmeted head without facemask. Under rear impact, compared with helmeted head without facemask, acceleration impulse reached to the peak smoothly.

### 4.4.3 Relationship between helmet dimension change and brain response

Generally, the helmet length/width aspect ratio was different as impact location changes. The highest aspect ratio was induced by rear impact, followed by frontal impact, while frontal boss impact produced the lowest aspect ratio. Under rear impact, facemask decreased helmet dimension largely, which induced high length/width aspect ratio. Under frontal boss impact, the dimension of the helmet with and without facemask didn't change much, which induced low length/width aspect ratio. When comparing a helmet with a facemask to one without, an observation that the dimension change of helmet with a facemask was reduced under frontal impact, lateral impact, rear boss impact and facemask impact (Table 4.1). As the stiffness of the helmet is increased by the facemask [64], the dimension change of the helmet with facemask is expected to be smaller.

Under frontal impact and lateral impact, the removal of the facemask increased brain strain distribution because more impact energy was transferred to the head due to the lower stiffness. Under the frontal boss impact, the dimension of the helmet with and without the facemask did not have significant changes (less than 3%), which induced similar brain strain distribution change (less than 3%). Although the dimension change of the helmet with facemask was larger, the brain distribution was decreased by including the facemask because the facemask attempts to retain the helmet shape, which constrains the impactors. Under the impact to the facemask (to the lateral zygoma), although dimension changes of helmet with and without facemask were similar, the facemask increased brain strain distribution. This is expected as the facemask acted as a longer moment arm, increasing axial rotation.

### 4.4.4 Limitation

This study has some limitations that need to be taken into consideration, especially when considering the FE model. One limitation is that the neck muscles in these simulations were treated as passive muscles meaning that they were reacting to the impact. In some real-world impact scenarios, the muscles of the neck would be acting in an active matter meaning that they would be expecting and engaged before the impact. A second limitation

is that while the head model and the helmet model have each been validated individually, there is currently no validation for their combined use.

## 4.5 Conclusion

Our study found that the influence of the facemask was dependent on the impact location. The removal of the facemask induced more helmet dimension change after the impact in general, which influenced brain strain distribution results. The facemask adds an increased rigidity to the helmet, this increased rigidity shows effects on the helmet length to width aspect ratio. The inclusion of the facemask also showed to increase the intracranial pressures in the brain in the form of coup and contre-coup pressures. These results seem to indicate that future helmet testing must be undertaken with the presence of a facemask, and that there needs to be more focused research on the effects of a facemask in brain response rather than just as a method in reducing facial injuries. The acceleration impulse was different as the inclusion of facemask under lateral and rear impact. Equipment manufacturers are advised to look into how to optimize facemask to reduce brain injury, besides protecting facial structures.

# Chapter 5

# 5 Conclusion and future work

## 5.1 Conclusion

### 5.1.1 Brain injury prediction

Head linear and rotational accelerations do not directly correlate to brain injury. These accelerations induce brain mechanical responses that are directly linked to injury. To explore appropriate kinematic predictor to predict the brain injury, the study systemically investigated the correlation between head kinematics to brain strain response. Generally, compared to the peak acceleration that is commonly used to evaluate brain injury risk, peak rotational velocity correlated better to brain strain distribution under the short impact duration relevant to sports concussions.

Impact directions influenced brain strain. Axial rotation produced highest strain to the whole brain while lateral bending produced lowest strain. Meanwhile, the same lateral bending produced highest strain to the corpus callosum and the thalamus. Flexion and extension induced similar, middle-level strains to the whole brain while they produced highest strains to the basal ganglia. These various effects of impact direction on the whole-brain and deep-brain structures are critical to concussion prediction and prevention as deep brain structures have been reported to be concussion relevant.

Rotation was demonstrated as the main reason to induce brain strain. The effect of linear motion on brain strain could be neglected.

Deceleration can’t be ignored when head kinematic curves were collected. When deceleration duration was less than 10 ms, brain strain distribution result was reduced by 17%. Brain strain distribution result was increased up to 30% when deceleration duration reached to 30 ms.

The impact loading curve shape was also demonstrated to affect brain strain distribution result. Based on the same peak rotational acceleration, rectangular loading curve

produced the highest brain strain distribution result, while the triangular loading curve induced the lowest brain strain distribution result.

### 5.1.2 Brain protection

The football helmet could protect the brain by largely reducing brain strain distribution and brain pressure because part of impact energy acting on the helmet was absorbed. The contribution of helmet part to energy absorption was different. Helmet shell absorbed around half of the energy, followed by the foams which were close to the impact locations. Hence, optimization of both the hard shell and foam pad to was found to be critical to reduce brain strains.

The football facemask did affect the brain response. The removal of the facemask induced more helmet dimension change than the helmet with the facemask did. The facemask added rigidity to the helmet. This increased rigidity showed effects on the helmet's length to width aspect ratio. The facemask also increased the intracranial pressures in the brain in the form of coup and contrecoup pressures.

## 5.2 Limitation

The neck model used in this study was based on the passive neck material without muscle activation. The neck could be activated when the head is impacted, which may induce different brain response. It is acknowledged that the contribution of neck response was not considered.

There lacks a direct validation test when head & neck model and helmet model were combined in real human based on brain pressure, brain strain and brain displacement. However, the head & neck model was validated against the brain and neck response based on the cadaver tests. The helmet was also validated based on the physical dummy tests. Since the same loading and boundary conditions such as helmet to the scalp frictions were applied between helmet-on-human and helmet-on-dummy situations, it is justified that data presented in this study could be accepted while the limitation of lack of direct validation needs to be acknowledged.

## 5.3 Future study

The findings from this stud provide enormous opportunities for future research in terms better predicting and preventing TBI.

### 5.3.1 The Traumatic brain injury mechanisms

As both animal and human brain involving neuron cells, axons and blood vessels have the similar material properties, the injury rationale being investigated based on animal can be transferred to human brain injury studied. To further investigate the mechanism of TBI, the controlled and measurable animal experiment will be used. Hence, laboratory animal studies that can reasonably mimic real-world head impact biomechanics are strongly recommended.

### 5.3.2 Brain injury predicators

Based on the football-related impacts, head peak rotational velocity was correlated closely to brain strain distribution. However, whether head peak rotational velocity will still correlate to brain strain distribution closely during other sports-related impacts with long impact duration (more than 50 ms) was not investigated in this study. The correlation between head peak rotational velocity and brain strain distribution under longer-duration impact such as boxing will be investigated in the future.

### 5.3.3 Brain response validation

The head & neck model with helmet will be validated against the human brain response under impact velocity (with different directions) which is safe to human brain.

### 5.3.4 Helmet design optimization

The optimization of helmet design is the critical to improve the brain protection efficiency. In the future, helmet structure design will be improved in three aspects: (1) improve the shell structure by exploring the effect of shell (with different material properties) on brain response; (2) improve foam design by investigating the effect of foam on brain response; (3) optimize combination of shell and foam with proper material property that can protect

the brain effectively; (4) evaluate the performance of helmets with different structure design.

#### 5.3.4.1 The effect of shell

Helmet shell is critical because it absorbed around 50% of the energy. Hence, investigation of the effect of shell alone is the priority to optimize the helmet design. Initially, the preliminary study indicated that as young's modulus changed, brain strain distribution varied nonlinearly (Figure 5.1). However, the mechanism about how shell material property influences the brain response is unknown. The in-depth study will be executed to evaluate how helmet shell material property affects brain response.

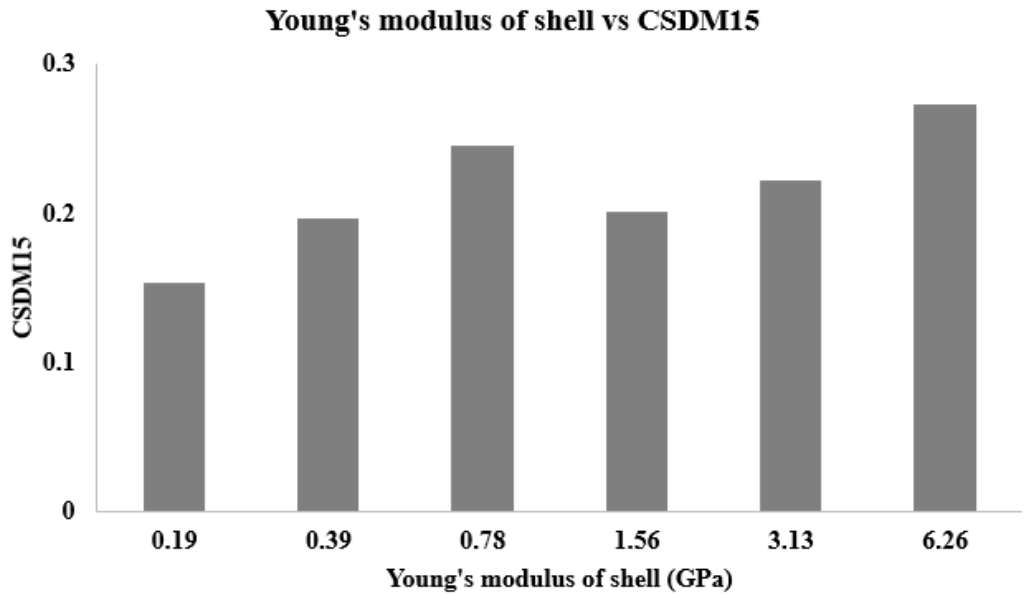


**Figure 5.1 The effect of shell.**

#### 5.3.4.2 The effect of foam

The foams close to impact locations contributed to the impact energy absorption, which reduced brain strain distribution result. Both the shape and material property of foam can affect the performance. However, effect of foam shape and material property is unclear. Based on the design of experiment, the effect of foam shape and material properties on the brain response will be evaluated.

#### 5.3.4.3 Optimization of shell and foam combination

Based on shell and foam study, the effect of helmet shell and foam on brain response will be identified. However, there lacks a study about how will both shell and foams cooperate to affect the brain response. An experiment with different combinations of shell (with different material properties) and foams (with different shapes and material properties) will be designed to evaluate how helmet shell and foam cooperate to affect brain response. Moreover, best combination of shell and foams that induced less brain response will be optimized.

### 5.3.5 The performance of other helmets

As helmet performance varies as helmet structure design changed, evaluating the effectiveness of different helmets is needed. Except Riddell Speed Classic helmet, there are other commonly used helmets including Schutt Air XP Pro helmet, Xenith X2E helmet and Vicis Zero1 football helmets. These helmets have different structural designs of outer shell, foams and facemask. The performance of Schutt Air XP Pro helmet, Xenith X2E helmet and Vicis Zero1 will be evaluated based on brain responses.

## 5.4 Significance and novelty

The direct and conventional way to evaluate brain injury risk is to predict injury based on head kinematics. However, there lacks a study to systematically investigate the correlation between head kinematics and brain strain response that directly links to neuronal damage, which was addressed in this study.

Peak rotational velocity was found to be a good predictor for brain injury, as it correlated to brain strain distribution closely. The traditionally used peak rotational acceleration didn’t always correlate to brain strain, with its accuracy being affected by impact duration time. Hence, it is recommended to highlight peak rotational velocity for future brain injury criteria.

Impact directions affected the whole brain and deep-brain components differently. Moreover, impact kinematic factors, including loading curve shapes and deceleration, were demonstrated to affect brain strain response. In the long term, developing and adopting FE-based brain injury criteria that can take account of the aforementioned effects is recommended. Meanwhile, direction-specific concussion injuries need to be correlated to direction-specific brain biomechanics.

Wearing helmet was regarded as an effective way to reduce the risk of brain injury. Currently, helmets are evaluated based on the dummy head kinematic response, rather than the brain response. The performance of helmet to protect brain was dependent on helmet design. Understand the helmet protection mechanism is critical to optimize the helmet design to better protect brain effectively. However, there lacks a study to systematically investigate the helmet protection mechanism.

Helmet reduced the brain injury risk by decreasing brain strain distribution and intracranial pressure. Interestingly, by evaluating the energy absorption ratio contributed by each helmet parts, around half of the energy was absorbed by the helmet shell, followed by the foams close to impact locations. While the traditional approach has been focused on optimizing foam pads to absorb impact energy, the role of helmet shell has been underestimated, and needs to be further investigated in the future.

Facemask increased intracranial pressure, but the facemask’s effect on strain varied as impact location changed. In general, facemask increased helmet rigidity and hence caused high correlation between helmet length to width aspect ratio and brain strain change.

# References or Bibliography


[1] Biocore. *Biocore, LLC*. Available: www.biocorellc.com

[2] P. J. McMahon *et al.*, "Symptomatology and functional outcome in mild traumatic brain injury: results from the prospective TRACK-TBI study," vol. 31, no. 1, pp. 26-33, 2014.

[3] J. A. Langlois, W. Rutland-Brown, and M. M. Wald, "The epidemiology and impact of traumatic brain injury: a brief overview," *The Journal of head trauma rehabilitation*, vol. 21, no. 5, pp. 375-378, 2006.

[4] J. F. Malec *et al.*, "The mayo classification system for traumatic brain injury severity," vol. 24, no. 9, pp. 1417-1424, 2007.

[5] K. M. Guskiewicz *et al.*, "Recurrent concussion and risk of depression in retired professional football players," vol. 39, no. 6, p. 903, 2007.

[6] P. McCrory *et al.*, "Consensus statement on Concussion in Sport–the 3rd International Conference on Concussion in Sport held in Zurich, November 2008," vol. 21, no. 2, 2009.

[7] N. J. Brown, R. C. Mannix, M. J. O'Brien, D. Gostine, M. W. Collins, and W. P. Meehan III, "Effect of cognitive activity level on duration of post-concussion symptoms," *Pediatrics*, vol. 133, no. 2, p. e299, 2014.

[8] K. Dams-O'Connor, L. E. Gibbons, J. D. Bowen, S. M. McCurry, E. B. Larson, and P. K. Crane, "Risk for late-life re-injury, dementia and death among individuals with traumatic brain injury: a population-based study," *J Neurol Neurosurg Psychiatry*, vol. 84, no. 2, pp. 177-182, 2013.

[9] M. McCrea, T. Hammeke, G. Olsen, P. Leo, and K. Guskiewicz, "Unreported concussion in high school football players: implications for prevention," *Clinical journal of sport medicine*, vol. 14, no. 1, pp. 13-17, 2004.

[10] A. C. McKee *et al.*, "Chronic traumatic encephalopathy in athletes: progressive tauopathy after repetitive head injury," *Journal of Neuropathology Experimental Neurology*, vol. 68, no. 7, pp. 709-735, 2009.

[11] H. Mao, "Modeling the head for impact scenarios," in *Basic Finite Element Method as Applied to Injury Biomechanics*: Elsevier, 2018, pp. 469-502.

[12] B. Kolb and I. Q. Whishaw, *Fundamentals of human neuropsychology*. Macmillan, 2009.

[13] E. Skoe, J. Krizman, S. Anderson, and N. Kraus, "Stability and plasticity of auditory brainstem function across the lifespan," *Cerebral Cortex,* vol. 25, no. 6, pp. 1415-1426, 2013.

[14] D. L. Sparks, "The brainstem control of saccadic eye movements," *Nature Reviews Neuroscience,* vol. 3, no. 12, p. 952, 2002.

[15] J. A. Hobson, R. W. McCarley, and P. W. Wyzinski, "Sleep cycle oscillation: reciprocal discharge by two brainstem neuronal groups," *Science,* vol. 189, no. 4196, pp. 55-58, 1975.

[16] R. L. West, "An application of prefrontal cortex function theory to cognitive aging," *Psychological bulletin,* vol. 120, no. 2, p. 272, 1996.

[17] L. K. Paul *et al.*, "Agenesis of the corpus callosum: genetic, developmental and functional aspects of connectivity," *Nature Reviews Neuroscience,* vol. 8, no. 4, p. 287, 2007.

[18] S. M. Sherman and R. W. Guillery, *Exploring the thalamus and its role in cortical function*. MIT press, 2006.

[19] A. M. Graybiel, "The basal ganglia," *Current Biology,* vol. 10, no. 14, pp. R509-R511, 2000.

[20] M. Allin *et al.*, "Cognitive and motor function and the size of the cerebellum in adolescents born very pre-term," *Brain,* vol. 124, no. 1, pp. 60-66, 2001.

[21] O. College. (2013). *Lateral View of Skull*. Available: https://commons.wikimedia.org/wiki/File:705_Lateral_View_of_Skull-01.jpg

[22] J. M. Meythaler, J. D. Peduzzi, E. Eleftheriou, and T. A. Novack, "Current concepts: diffuse axonal injury–associated traumatic brain injury," *Archives of physical medicine rehabilitation,* vol. 82, no. 10, pp. 1461-1471, 2001.

[23] K. M. Guskiewicz and J. P. Mihalik, "Biomechanics of Sport Concussion: Quest for the Elusive Injury Threshold," (in English), *Exercise and Sport Sciences Reviews,* Review vol. 39, no. 1, pp. 4-11, Jan 2011.

[24] S. Ji *et al.*, "Group-wise evaluation and comparison of white matter fiber strain and maximum principal strain in sports-related concussion," *Journal of neurotrauma,* vol. 32, no. 7, pp. 441-454, 2015.

[25] S. Kleiven, "Predictors for traumatic brain injuries evaluated through accident reconstructions," SAE Technical Paper2007.

[26] E. J. Sanchez, L. F. Gabler, A. B. Good, J. R. Funk, J. R. Crandall, and M. B. Panzer, "A reanalysis of football impact reconstructions for head kinematics and finite element modeling," (in eng), *Clin Biomech (Bristol, Avon),* Mar 14 2018.

[27] E. J. Pellman, D. C. Viano, A. M. Tucker, I. R. Casson, and J. F. Waeckerle, "Concussion in professional football: reconstruction of game impacts and injuries," (in eng), *Neurosurgery,* vol. 53, no. 4, pp. 799-812; discussion 812-4, Oct 2003.

[28] D. C. Viano, E. J. Pellman, C. Withnall, and N. Shewchenko, "Concussion in professional football: performance of newer helmets in reconstructed game impacts—part 13," *Neurosurgery,* vol. 59, no. 3, pp. 591-606, 2006.

[29] L. Zhang, K. H. Yang, and A. I. King, "A proposed injury threshold for mild traumatic brain injury," (in eng), *J Biomech Eng,* vol. 126, no. 2, pp. 226-36, Apr 2004.

[30] S. S. Margulies and L. E. Thibault, "A proposed tolerance criterion for diffuse axonal injury in man," (in English), *Journal of Biomechanics,* Article vol. 25, no. 8, pp. 917-923, Aug 1992.

[31] H. Kimpara and M. Iwamoto, "Mild traumatic brain injury predictors based on angular accelerations during impacts," *Annals of biomedical engineering,* vol. 40, no. 1, pp. 114-126, 2012.

[32] E. G. Takhounts, M. J. Craig, K. Moorhouse, J. McFadden, and V. Hasija, "Development of brain injury criteria (BrIC)," *Stapp car crash journal,* vol. 57, p. 243, 2013.

[33] J. Hutchinson, M. J. Kaiser, and H. M. Lankarani, "The head injury criterion (HIC) functional," *Applied mathematics and computation,* vol. 96, no. 1, pp. 1-16, 1998.

[34] J. Newman *et al.*, "A new biomechanical assessment of mild traumatic brain injury. Part 2: results and conclusions," in *Proceedings of the International Research Council on the Biomechanics of Injury conference*, 2000, vol. 28: International Research Council on Biomechanics of Injury.

[35] J. A. Newman, "A generalized acceleration model for brain injury threshold (GAMBIT)," in *Proceedings of International IRCOBI Conference, 1986,* 1986.

[36] H. Mao *et al.*, "Development of a finite element human head model partially validated with thirty five experimental cases," *Journal of biomechanical engineering,* vol. 135, no. 11, p. 111002, 2013.

[37] L. Zhang *et al.*, "Recent advances in brain injury research: a new human head model development and validation," SAE Technical Paper2001.

[38] H.-S. Kang, R. Willinger, B. M. Diaw, and B. Chinn, "Validation of a 3D anatomic human head model and replication of head impact in motorcycle accident by finite element modeling," *SAE transactions,* pp. 3849-3858, 1997.

[39] J. S. Raul, C. Deck, R. Willinger, and B. Ludes, "Finite-element models of the human head and their applications in forensic practice," *International journal of legal medicine,* vol. 122, no. 5, pp. 359-366, 2008.

[40] S. Kleiven and H. von Holst, "Consequences of brain size following impact in prediction of subdural hematoma evaluated with numerical techniques," in *Proceedings of the International Conference on the Biomechanics of Impact (IRCOBI'01),* 2001, pp. 161-172.

[41] E. G. Takhounts, R. H. Eppinger, J. Q. Campbell, and R. E. Tannous, "On the development of the SIMon finite element head model," *Stapp car crash journal,* vol. 47, p. 107, 2003.

[42] D. A. Patton, A. S. McIntosh, and S. Kleiven, "The biomechanical determinants of concussion: finite element simulations to investigate brain tissue deformations during sporting impacts to the unprotected head," *Journal of applied biomechanics,* vol. 29, no. 6, pp. 721-730, 2013.

[43] T. W. McAllister *et al.*, "Maximum principal strain and strain rate associated with concussion diagnosis correlates with changes in corpus callosum white matter indices," *Annals of biomedical engineering,* vol. 40, no. 1, pp. 127-140, 2012.

[44] D. C. Viano, I. R. Casson, E. J. Pellman, L. Zhang, A. I. King, and K. H. Yang, "Concussion in professional football: brain responses by finite element analysis: part 9," *Neurosurgery,* vol. 57, no. 5, pp. 891-916, 2005.

[45] N. Yoganandan, J. Li, J. Zhang, F. A. Pintar, and T. A. Gennarelli, "Influence of angular acceleration–deceleration pulse shapes on regional brain strains," *Journal of biomechanics,* vol. 41, no. 10, pp. 2253-2262, 2008.

[46] W. Zhao and S. Ji, "Brain strain uncertainty due to shape variation in and simplification of head angular velocity profiles," *Biomechanics and modeling in mechanobiology,* vol. 16, no. 2, pp. 449-461, 2017.

[47] A. Post, T. B. Hoshizaki, M. D. Gilchrist, and M. D. Cusimano, "Peak linear and rotational acceleration magnitude and duration effects on maximum principal strain in the corpus callosum for sport impacts," *Journal of biomechanics,* vol. 61, pp. 183-192, 2017.

[48] B. S. Elkin, L. F. Gabler, M. B. Panzer, and G. P. Siegmund, "Brain tissue strains vary with head impact location: A possible explanation for increased concussion risk in struck versus striking football players," *Clinical biomechanics,* 2018.

[49] L. Zhang, K. H. Yang, and A. I. King, "Comparison of brain responses between frontal and lateral impacts by finite element modeling," *Journal of neurotrauma,* vol. 18, no. 1, pp. 21-30, 2001.

[50] R. C. Cantu, *Neurologic athletic head and spine injuries*. WB Saunders Company, 2000.

[51] S. Rowson *et al.*, "Can helmet design reduce the risk of concussion in football?," *Journal of neurosurgery,* vol. 120, no. 4, pp. 919-922, 2014.

[52] A. Trotta, D. Zouzias, G. De Bruyne, and A. N. Annaidh, "The importance of the scalp in head impact kinematics," *Annals of biomedical engineering,* vol. 46, no. 6, pp. 831-840, 2018.

[53] D. C. Viano, C. Withnall, and D. Halstead, "Impact performance of modern football helmets," *Annals of biomedical engineering,* vol. 40, no. 1, pp. 160-174, 2012.

[54] J. F. Kraus, B. D. Anderson, and C. Mueller, "The effectiveness of a special ice hockey helmet to reduce head injuries in college intramural hockey," *Medicine science in sports,* vol. 2, no. 3, pp. 162-164, 1970.

[55] Andy. (2009). *Stylized image of a Pittsburgh Steelers helmet sitting on a grass field*. Available: https://commons.wikimedia.org/wiki/File:Steelers_helmet_on_grass_field.jpg

[56] T. B. Hoshizaki and S. E. Brien, "The science and design of head protection in sport," *Neurosurgery,* vol. 55, no. 4, pp. 956-967, 2004.

[57] C. W. Gadd, "Use of a weighted-impulse criterion for estimating injury hazard," SAE Technical Paper0148-7191, 1966.

[58] J. A. Newman, "Head injury criteria in automotive crash testing," *SAE Transactions,* pp. 4098-4115, 1980.

[59] A. Post, A. Oeur, E. Walsh, B. Hoshizaki, and M. D. Gilchrist, "A centric/non-centric impact protocol and finite element model methodology for the evaluation of American football helmets to evaluate risk of concussion," *Computer methods in biomechanics and biomedical engineering,* vol. 17, no. 16, pp. 1785-1800, 2014.

[60] T. B. Hoshizaki, A. Post, R. A. Oeur, and S. E. Brien, "Current and future concepts in helmet and sports injury prevention," *Neurosurgery,* vol. 75, no. suppl_4, pp. S136-S148, 2014.

[61] H. Joodaki, A. Bailey, D. Lessley, J. Funk, C. Sherwood, and J. Crandall, "Relative motion between the helmet and head in football impact test," *Journal of biomechanical engineering,* 2019.

[62] A. C. Bain and D. F. Meaney, "Tissue-level thresholds for axonal damage in an experimental model of central nervous system white matter injury," *Journal of biomechanical engineering,* vol. 122, no. 6, pp. 615-622, 2000.

[63] K. M. Breedlove, E. L. Breedlove, T. G. Bowman, E. M. Arruda, and E. A. Nauman, "The effect of football helmet facemasks on impact behavior during linear drop tests," *Journal of biomechanics,* vol. 79, pp. 227-231, 2018.

[64] G. A. Rush *et al.*, "Comparison of shell-facemask responses in American football helmets during NOCSAE drop tests," vol. 20, no. 3, pp. 199-211, 2017.

[65] B. Rowson, E. J. Terrell, and S. Rowson, "Quantifying the effect of the facemask on helmet performance," *Proceedings of the Institution of Mechanical Engineers, Part P: Journal of Sports Engineering Technology*, vol. 232, no. 2, pp. 94-101, 2018.

[66] C. Mac Donald, K. Dikranian, S. Song, P. Bayly, D. Holtzman, and D. Brody, "Detection of traumatic axonal injury with diffusion tensor imaging in a mouse model of traumatic brain injury," *Experimental neurology,* vol. 205, no. 1, pp. 116-131, 2007.

[67] D. H. Smith, X.-H. Chen, B.-N. Xu, T. K. McIntosh, T. A. Gennarelli, and D. E. Meaney, "Characterization of diffuse axonal pathology and selective hippocampal damage following inertial brain trauma in the pig," *Journal of Neuropathology & Experimental Neurology,* vol. 56, no. 7, pp. 822-834, 1997.

[68] Y. Zhang *et al.*, "Cerebrolysin Reduces Astrogliosis and Axonal Injury and Enhances Neurogenesis in Rats After Closed Head Injury," *Neurorehabilitation neural repair,* vol. 33, no. 1, pp. 15-26, 2019.

[69] Y. M. Morozov, Y. Y. Sun, C. Y. Kuan, and P. Rakic, "Alteration of SLP 2‐like immunolabeling in mitochondria signifies early cellular damage in developing and adult mouse brain," *European Journal of Neuroscience,* vol. 43, no. 2, pp. 245-257, 2016.

[70] C.-C. Chiu *et al.*, "Neuroinflammation in animal models of traumatic brain injury," *Journal of neuroscience methods,* vol. 272, pp. 38-49, 2016.

[71] H. L. Cater, L. E. Sundstrom, and B. Morrison III, "Temporal development of hippocampal cell death is dependent on tissue strain but not strain rate," *Journal of biomechanics,* vol. 39, no. 15, pp. 2810-2818, 2006.

[72] B. Morrison III, H. L. Cater, C. D. Benham, and L. E. Sundstrom, "An in vitro model of traumatic brain injury utilising two-dimensional stretch of organotypic hippocampal slice cultures," *Journal of neuroscience methods,* vol. 150, no. 2, pp. 192-201, 2006.

[73] V. S. S. S. Sajja *et al.*, "Blast‐induced neurotrauma leads to neurochemical changes and neuronal degeneration in the rat hippocampus," *NMR in biomedicine,* vol. 25, no. 12, pp. 1331-1339, 2012.

[74] R. D. Readnower *et al.*, "Increase in blood‐brain barrier permeability, oxidative stress, and activated microglia in a rat model of blast‐induced traumatic brain injury," *Journal of neuroscience research,* vol. 88, no. 16, pp. 3530-3539, 2010.

[75] A. Post, B. Hoshizaki, and M. D. Gilchrist, "Finite element analysis of the effect of loading curve shape on brain injury predictors," (in eng), *J Biomech,* vol. 45, no. 4, pp. 679-83, Feb 23 2012.

[76] S. Rowson *et al.*, "Rotational Head Kinematics in Football Impacts: An Injury Risk Function for Concussion," (in English), *Annals of Biomedical Engineering,* Article vol. 40, no. 1, pp. 1-13, Jan 2012.

[77] T. B. Hoshizaki *et al.*, "The development of a threshold curve for the understanding of concussion in sport," *Trauma,* vol. 19, no. 3, pp. 196-206, 2017.

[78] E. J. Pellman, D. C. Viano, A. M. Tucker, and I. R. Casson, "Concussion in professional football: Location and direction of helmet impacts—Part 2," *Neurosurgery,* vol. 53, no. 6, pp. 1328-1341, 2003.

[79] J. G. Beckwith *et al.*, "Timing of Concussion Diagnosis Is Related to Head Impact Exposure Prior to Injury," (in English), *Medicine and Science in Sports and Exercise,* Article vol. 45, no. 4, pp. 747-754, Apr 2013.

[80] R. M. Greenwald, J. T. Gwin, J. J. Chu, and J. J. Crisco, "Head impact severity measures for evaluating mild traumatic brain injury risk exposure," (in English), *Neurosurgery,* Article vol. 62, no. 4, pp. 789-798, Apr 2008.

[81] S. Rowson, G. Brolinson, M. Goforth, D. Dietter, and S. Duma, "Linear and Angular Head Acceleration Measurements in Collegiate Football," (in English), *Journal of Biomechanical Engineering-Transactions of the Asme,* Article vol. 131, no. 6, p. 7, Jun 2009, Art. no. 061016.

[82] D. C. Viano and E. J. Pellman, "Concussion in professional football: Biomechanics of the striking player - Part 8," (in English), *Neurosurgery,* Article vol. 56, no. 2, pp. 266-278, Feb 2005.

[83] L. E. Thibault, T. A. Gennarelli, S. S. Margulies, J. Marcus, and R. Eppinger, "The strain dependent pathophysiological consequences of inertial loading on central nervous system tissue," in *International Conference on the Biomechanics of Impacts, Bron,* 1990.

[84] D. I. Shreiber, A. C. Bain, and D. F. Meaney, "In vivo thresholds for mechanical injury to the blood-brain barrier," SAE Technical Paper0148-7191, 1997.

[85] D. C. Viano and P. Lovsund, "Biomechanics of brain and spinal-cord injury: analysis of neuropathologic and neurophysiology experiments," *Traffic Injury Prevention,* vol. 1, no. 1, pp. 35-43, 1999.

[86] A. I. King, K. H. Yang, L. Zhang, W. Hardy, and D. C. Viano, "Is head injury caused by linear or angular acceleration," in *IRCOBI conference*, 2003, pp. 1-12: Lisbon, Portugal.

[87] E. G. Takhounts *et al.*, "Investigation of traumatic brain injuries using the next generation of simulated injury monitor (SIMon) finite element head model," SAE Technical Paper2008.

[88] E. Chamard, G. Lefebvre, M. Lassonde, and H. Theoret, "Long-term abnormalities in the corpus callosum of female concussed athletes," *Journal of neurotrauma,* vol. 33, no. 13, pp. 1220-1226, 2016.

[89] E. J. Grossman and M. Inglese, "The role of thalamic damage in mild traumatic brain injury," *Journal of neurotrauma,* vol. 33, no. 2, pp. 163-167, 2016.

[90] L. Tang *et al.*, "Thalamic resting-state functional networks: disruption in patients with mild traumatic brain injury," *Radiology,* vol. 260, no. 3, pp. 831-840, 2011.

[91] F. Hernandez *et al.*, "Lateral impacts correlate with falx cerebri displacement and corpus callosum trauma in sports-related concussions," pp. 1-19, 2019.

[92] B. S. Elkin, J. M. Elliott, and G. P. Siegmund, "Whiplash injury or concussion? A possible biomechanical explanation for concussion symptoms in some individuals following a rear-end collision," *Journal of orthopaedic & sports physical therapy,* vol. 46, no. 10, pp. 874-885, 2016.

[93] J. Newman *et al.*, "A new biomechanical assessment of mild traumatic brain injury. Part 1: Methodology," in *Proceedings of the International Research Conference on the Biomechanics of Impacts (IRCOBI),* 1999, pp. 17-36.

[94] W. N. Hardy *et al.*, "A study of the response of the human cadaver head to impact," *Stapp car crash journal,* vol. 51, p. 17, 2007.

[95] J. Versace, "A review of the severity index," SAE Technical Paper0148-7191, 1971.

[96] GHBMC, "User Manual: F05 Detailed Occupant Version 3.1 for LS-DYNA," L. Global Human Body Models Consortium, Ed., ed, 2016, p. 53.

[97] A. M. Nahum, R. Smith, and C. C. Ward, "Intracranial pressure dynamics during head impact," SAE Technical Paper0148-7191, 1977.

[98] X. Trosseille, C. Tarriere, F. Lavaste, F. Guillon, and A. Domont, "Development of a FEM of the human head according to a specific test protocol," SAE Technical Paper0148-7191, 1992.

[99] W. N. Hardy, C. D. Foster, M. J. Mason, K. H. Yang, A. I. King, and S. Tashman, "Investigation of head injury mechanisms using neutral density technology and high-speed biplanar X-ray," *Stapp car crash journal*, vol. 45, pp. 337-368, 2001.

[100] Ls-PrePost. Available: ftp://ftp.lstc.com/outgoing/lsprepost/

[101] LS-DYNA. Available: https://www.lstc.com/products/ls-dyna

[102] U. Krave, M. Al-Olama, and H.-A. Hansson, "Rotational acceleration closed head flexion trauma generates more extensive diffuse brain injury than extension trauma," *Journal of neurotrauma*, vol. 28, no. 1, pp. 57-70, 2011.

[103] S. Kleiven, "Influence of direction and duration of impacts to the human head evaluated using the finite element method," in *International IRCOBI Conference*, 2005.

[104] B. M. Knowles and C. R. Dennison, "Predicting Cumulative and Maximum Brain Strain Measures From HybridIII Head Kinematics: A Combined Laboratory Study and Post-Hoc Regression Analysis," *Annals of biomedical engineering*, vol. 45, no. 9, pp. 2146-2158, 2017.

[105] L. F. Gabler, H. Joodaki, J. R. Crandall, and M. B. Panzer, "Development of a single-degree-of-freedom mechanical model for predicting strain-based brain injury responses," *Journal of biomechanical engineering*, vol. 140, no. 3, p. 031002, 2018.

[106] T. Bennett, *The NFL's official encyclopedic history of professional football*. Macmillan, 1977.

[107] C. A. Emery *et al.*, "What strategies can be used to effectively reduce the risk of concussion in sport? A systematic review," *British journal of sports medicine*, vol. 51, no. 12, pp. 978-984, 2017.

[108] M. L. Levy, B. M. Ozgur, C. Berry, H. E. Aryan, and M. L. Apuzzo, "Birth and evolution of the football helmet," *Neurosurgery*, vol. 55, no. 3, pp. 656-662, 2004.

[109] J. Mayrose, "The effects of a mandatory motorcycle helmet law on helmet use and injury patterns among motorcyclist fatalities," *Journal of safety research*, vol. 39, no. 4, pp. 429-432, 2008.

[110] E. S. Phipps and C. E. Phipps, "Protective helmet," ed: Google Patents, 2016.

[111] D. Hastings, "Helmet shell structure," ed: Google Patents, 1998.

[112] F. Rappleyea, "Football helmet having sectional liner of energy absorbing material," ed: Google Patents, 1974.

[113] J. J. Summers and H. W. Austin, "Safety hat energy absorbing liner," ed: Google Patents, 1975.

[114] W. E. Lancellotti, "Sports helmet with face mask," ed: Google Patents, 1980.

[115] S. Rowson and S. M. Duma, "Development of the STAR evaluation system for football helmets: integrating player head impact exposure and risk of concussion," *Annals of biomedical engineering*, vol. 39, no. 8, pp. 2130-2140, 2011.

[116] B. Morrison *et al.*, "A tissue level tolerance criterion for living brain developed with an in vitro model of traumatic mechanical loading," SAE Technical Paper2003.

[117] B. Morrison, B. S. Elkin, J.-P. Dollé, and M. L. Yarmush, "In vitro models of traumatic brain injury," *Annual Review of Biomedical Engineering*, vol. 13, no. 1, pp. 91-126, 2011.

[118] R. M. Chesnut *et al.*, "A trial of intracranial-pressure monitoring in traumatic brain injury," *New England Journal of Medicine*, vol. 367, no. 26, pp. 2471-2481, 2012.

[119] L. A. Steiner *et al.*, "Continuous monitoring of cerebrovascular pressure reactivity allows determination of optimal cerebral perfusion pressure in patients with traumatic brain injury," *Critical care medicine*, vol. 30, no. 4, pp. 733-738, 2002.

[120] J. B. Barker, D. S. Cronin, and R. W. Nightingale, "Lower cervical spine motion segment computational model validation: kinematic and kinetic response for quasi-static and dynamic loading," *Journal of biomechanical engineering*, vol. 139, no. 6, p. 061009, 2017.

[121] W. Decker, B. Koya, M. L. Davis, and F. S. Gayzik, "Modular use of human body models of varying levels of complexity: Validation of head kinematics," *Traffic injury prevention*, vol. 18, no. sup1, pp. S155-S160, 2017.

[122] M. Fahlstedt, M. Arnesen, E. Jungstedt, and P. Halldin. (2018). *Finite Element Model of 2016 Riddell Speed Classic (Safety Equipment Institute model R41179) Version 1.0 for LS-DYNA*. Available: http://biocorellc.com/resources/

[123] K. K. J. Sebastian Giudice, Adrian Caudillo, Sayak Mukherjee, Matthew B. Panzer. (2018). *Finite Element Models of Helmet Assessment Tools (Hybrid III Head-Neck, NOCSAE Headform, Linear Impact, Pendulum Impact, Drop Impact) Version 1.0 for LS-DYNA*. Available: http://biocorellc.com/resources/

[124] NOCSAE. (2017). *Standard performance specification for newly manufactured football helmets*. Available: https://nocsae.org/wp-content/uploads/2019/04/ND002-17m19-Mfrd-FB-Helmets-Standard-Performance-005.pdf

[125] J. A. Newman, M. C. Beusenberg, N. Shewchenko, C. Withnall, and E. Fournier, "Verification of biomechanical methods employed in a comprehensive study of mild traumatic brain injury and the effectiveness of American football helmets," *J Journal of biomechanics*, vol. 38, no. 7, pp. 1469-1481, 2005.

[126] L. M. Lewis, R. Naunheim, J. Standeven, C. Lauryssen, C. Richter, and B. Jeffords, "Do football helmets reduce acceleration of impact in blunt head injuries?," *Academic Emergency Medicine,* vol. 8, no. 6, pp. 604-609, 2001.

[127] P. A. Cripton, D. M. Dressler, C. A. Stuart, C. R. Dennison, and D. Richards, "Bicycle helmets are highly effective at preventing head injury during head impact: Head-form accelerations and injury criteria for helmeted and unhelmeted impacts," *Accident Analysis & Prevention*, vol. 70, pp. 1-7, 2014.

[128] S. Tiernan and G. Byrne, "The effect of impact location on brain strain," *Brain injury*, vol. 33, no. 4, pp. 427-434, 2019.

[129] C. A. Taylor, J. M. Bell, M. J. Breiding, and L. Xu, "Traumatic brain injury–related emergency department visits, hospitalizations, and deaths—United States, 2007 and 2013," *MMWR Surveillance Summaries*, vol. 66, no. 9, p. 1, 2017.

[130] T. M. Murray and L. A. Livingston, "Hockey helmets, face masks, and injurious behavior," *Pediatrics*, vol. 95, no. 3, pp. 419-421, 1995.

[131] P. D. Reynen and W. G. Clancy Jr, "Cervical spine injury, hockey helmets, and face masks," *The American journal of sports medicine*, vol. 22, no. 2, pp. 167-170, 1994.

[132] K. Johnson *et al.*, "Constrained topological optimization of a football helmet facemask based on brain response," *Materials & Design*, vol. 111, pp. 108-118, 2016.

[133] L. Thomas, V. Roberts, and E. Gurdjian, "Experimental intracranial pressure gradients in the human skull," *Journal of neurology, neurosurgery, psychiatry*, vol. 29, no. 5, p. 404, 1966.

[134] T. A. Gennarelli, L. E. Thibault, J. H. Adams, D. I. Graham, C. J. Thompson, and R. P. Marcincin, "Diffuse axonal injury and traumatic coma in the primate," *Annals of Neurology: Official Journal of the American Neurological Association the Child Neurology Society*, vol. 12, no. 6, pp. 564-574, 1982.

[135] S. Kleiven, "Why most traumatic brain injuries are not caused by linear acceleration but skull fractures are," *Frontiers in bioengineering and biotechnology*, vol. 1, p. 15, 2013.

# Appendices

## Appendix A Material property of finite element model

### Table A.1 Material property of finite model [36]

| Brain component | Density ($kg/m^3$) | Bulk Modulus (GPa) | Short-time shear modulus (kPa) | Long-time shear modulus (kPa) | Material Type | Element Type | |
|---|---|---|---|---|---|---|---|
| Cerebrum gray | 1060 | 2.19 | 6 | 1.2 | Viscoelastic | Solid | |
| Celebellum | 1060 | 2.19 | 6 | 1.2 | Viscoelastic | Solid | |
| Thalamus | 1060 | 2.19 | 6 | 1.2 | Viscoelastic | Solid | |
| Brain stem | 1060 | 2.19 | 6 | 1.2 | Viscoelastic | Solid | |
| Basal ganglia | 1060 | 2.19 | 6 | 1.2 | Viscoelastic | Solid | |
| CSF | 1040 | 2.19 | 0.5 | 0.1 | Viscoelastic | Solid | |
| 3rd Ventricle | 1040 | 2.19 | 0.5 | 0.1 | Viscoelastic | Solid | |
| Corpus callosum | 1060 | 2.19 | 7.5 | 1.5 | Viscoelastic | Solid | |
| Cerebrum gray | 1060 | 2.19 | 7.5 | 1.5 | Viscoelastic | Solid | |
| Brain component | Density ($kg/m^3$) | Young's Modulus (GPa) | Poission's ratio | Material Type | Element Type | | |
| Dura | 1100 | 0.0315 | 0.35 | Elastic | Shell | | |
| Flax | 1100 | 0.0125 | 0.35 | Elastic | Shell | | |
| Pia | 1100 | 0.0125 | 0.35 | Elastic | Shell | | |
| Tentorium | 1100 | 0.0315 | 0.3 | Elastic | Shell | | |
| Arachnoid | 1100 | 0.012 | 0.35 | Elastic | Shell | | |
| Brain component | Density ($kg/m^3$) | Young's Modulus (GPa) | Poission's ratio | Yield stress | Tangent modulus (Gpa) | Material Type (Gpa) | Element Type |
| Bridging vein | 1130 | 0.03 | 0.48 | 0.00413 | 0.0122 | Linear elastic plasticity | Beam |
| Component | Density ($kg/m^3$) | Young's Modulus (GPa) | Poission's ratio | Yield stress | Tangent modulus (Gpa) | Material Type (Gpa) | Element Type |
| Skull Diploe | 1000 | 0.6 | 0.3 | 0.004 | 0.02 | Linear elastic plasticity | Solid |
| Skull Outer | 2100 | 10 | 0.25 | 0.09 | 0.5 | Linear elastic plasticity | Solid |
| Skull Inner | 2100 | 10 | 0.25 | 0.09 | 0.5 | Linear elastic plasticity | Solid |
| Component | Density ($kg/m^3$) | Bulk Modulus (GPa) | Short-time shear modulus (kPa) | Long-time shear modulus (kPa) | Material Type | Element Type | |
| Facial tissue | 1100 | 0.005 | 0.00034 | 0.00014 | Viscoelastic | Solid | |
| Scalp | 1100 | 0.02 | 0.0017 | 0.00068 | Viscoelastic | Solid | |

## Appendix B Results of the CSDM10, CSDM15, CSDM20, CSDM25, and CSDM30 for various peak accelerations and rotational directions.

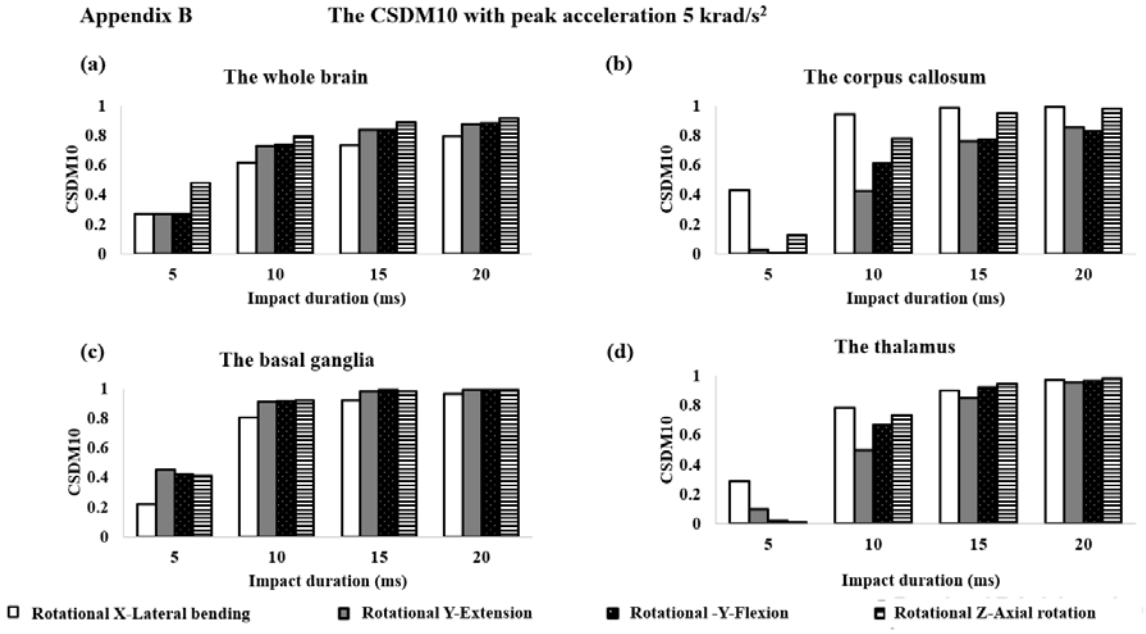


**Figure B.1 Results of the CSDM10 for peak acceleration 5 krad/s².**

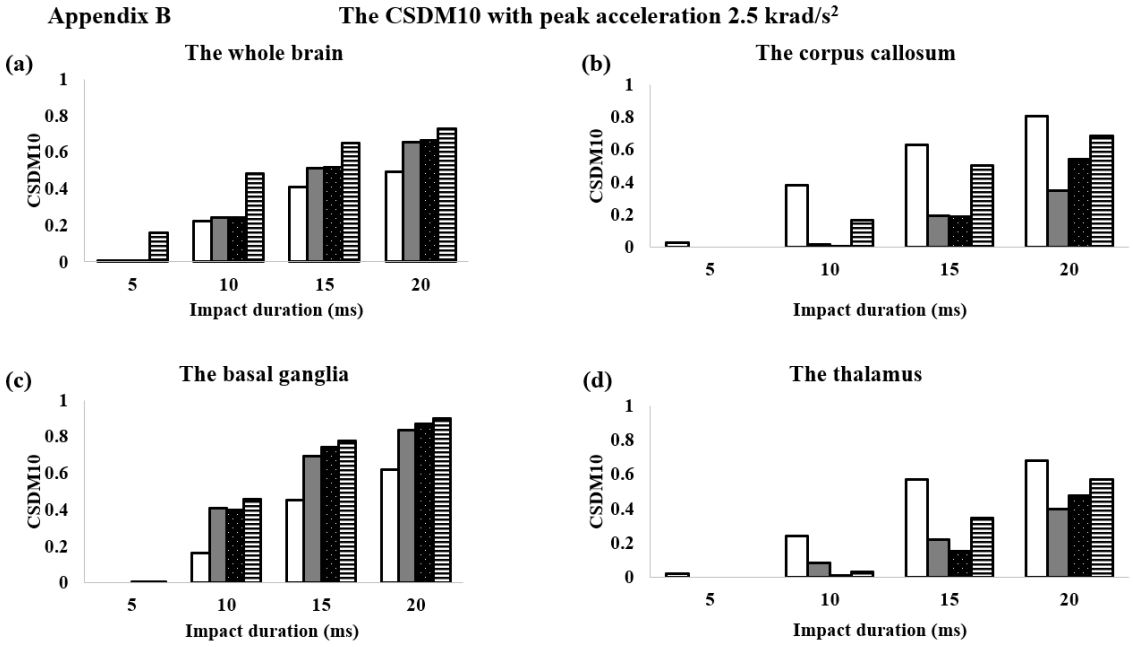


**Figure B.2 Results of the CSDM10 for peak acceleration 2.5 krad/s².**

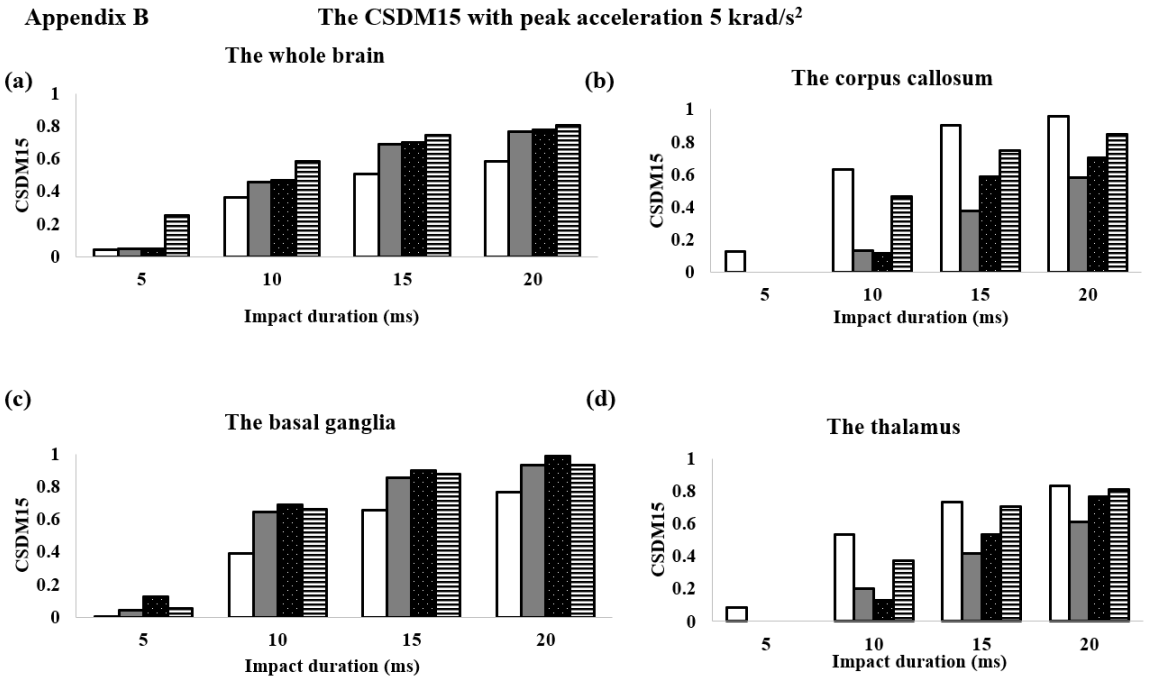


**Figure B.3 Results of the CSDM15 for peak acceleration 5 krad/s$^2$.**

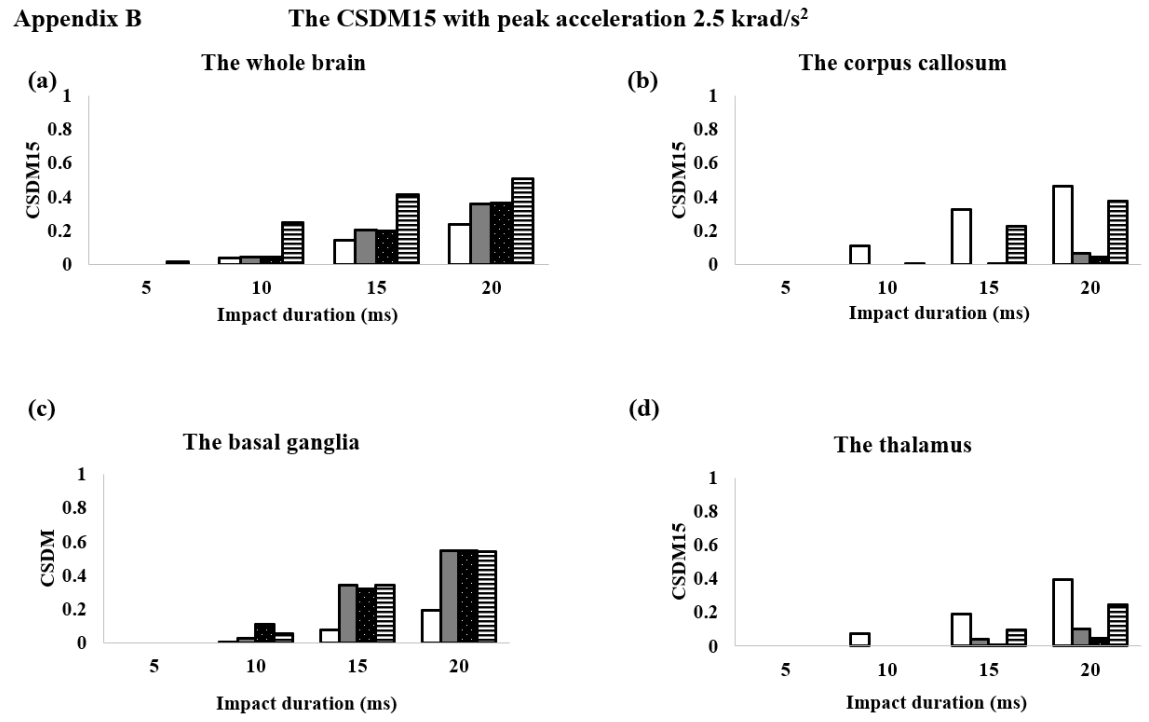


**Figure B.4 Results of the CSDM15 for peak acceleration 2.5 krad/s$^2$.**

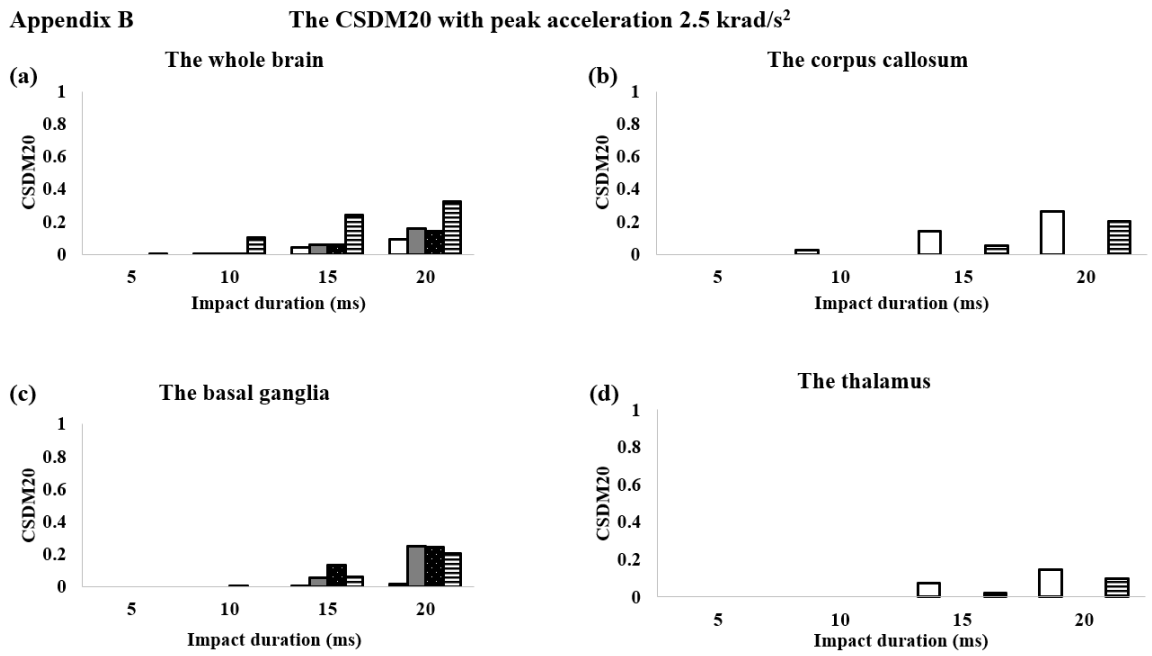


**Figure B.5 Results of the CSDM20 for peak acceleration 2.5 krad/s$^2$.**

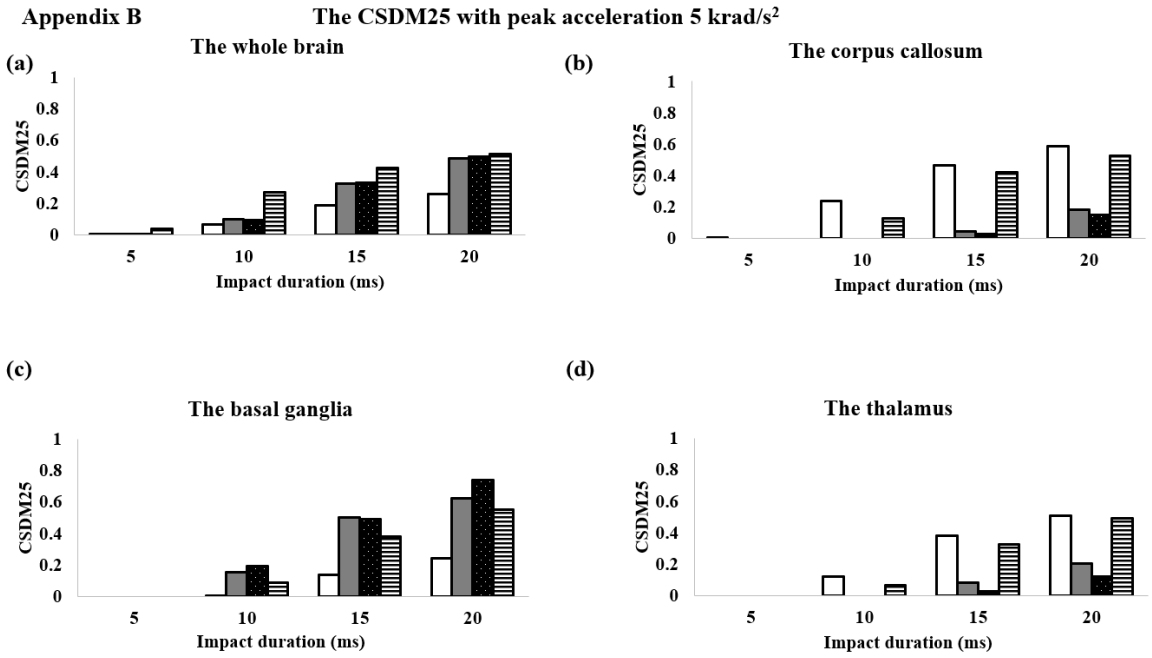


**Figure B.6 Results of the CSDM25 for peak acceleration 5 krad/s$^2$.**

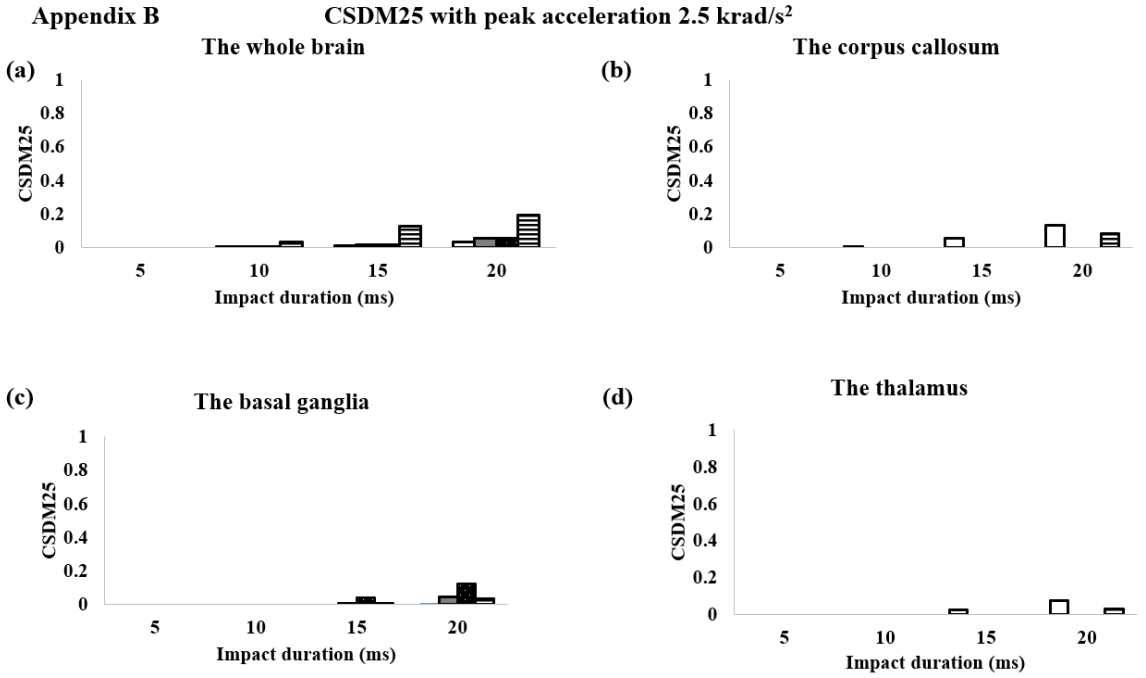


**Figure B.7 Results of the CSDM25 for peak acceleration 2.5 krad/s².**

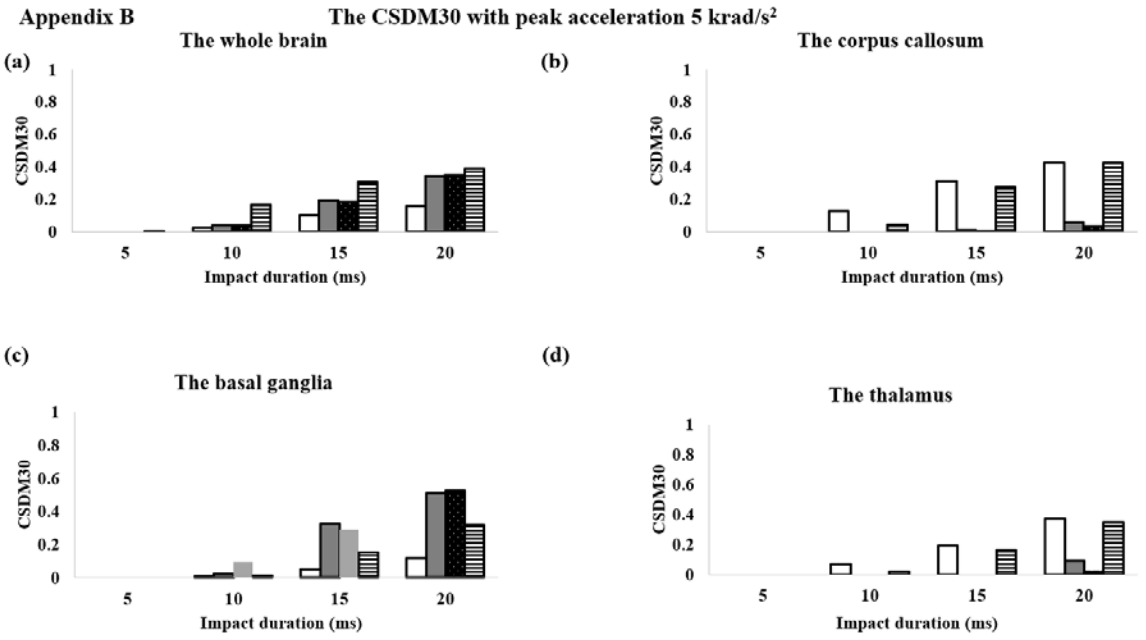


**Figure B.8 Results of the CSDM30 for peak acceleration 5 krad/s².**

Appendix B

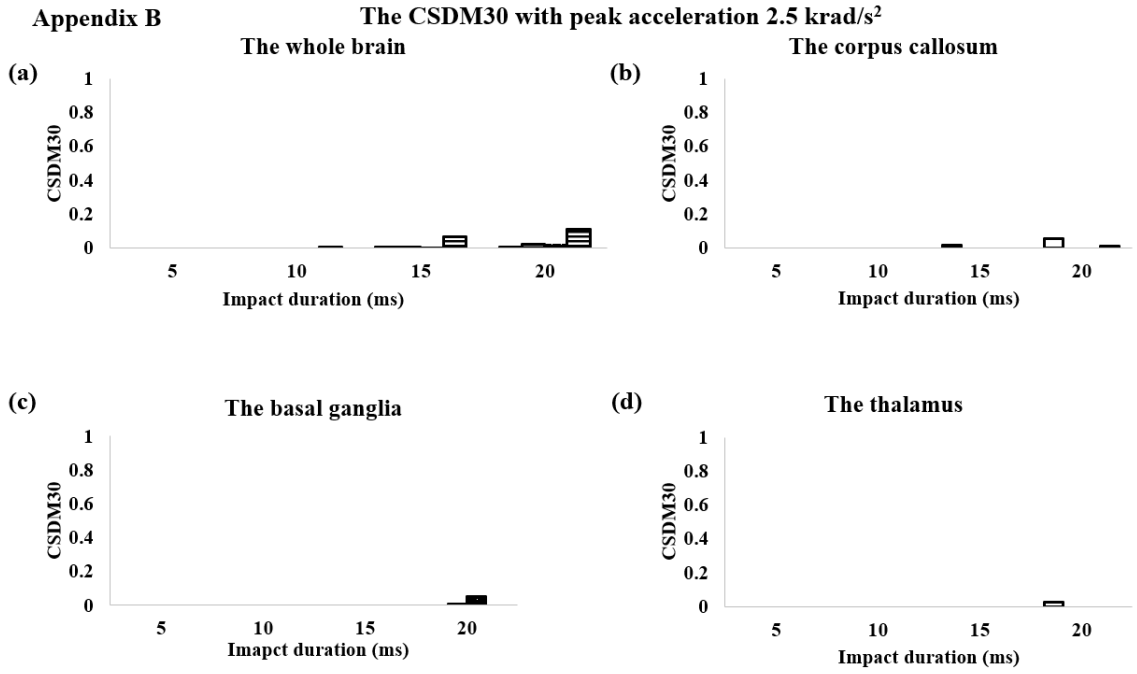


**Figure B.9 Results of the CSDM30 for peak acceleration 2.5 krad/s$^2$.**

## Appendix C The effects of deceleration.

**Appendix C** **The effects of deceleration**

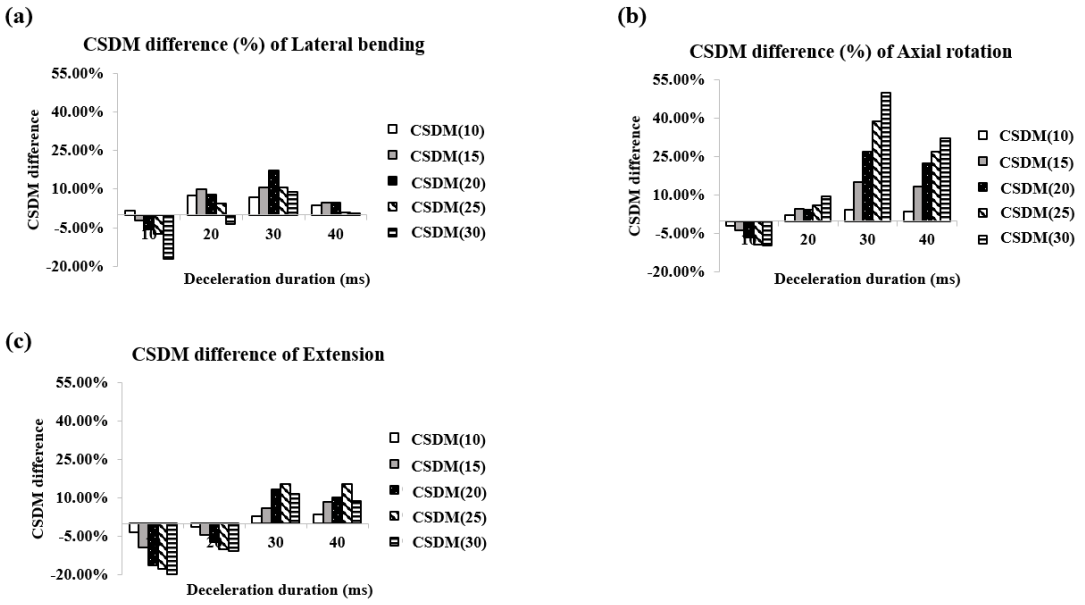


**Figure C.1 The CSDM difference of deceleration under lateral bending, lateral rotation. and extension.**

**Appendix D** **CSDM as a function of peak velocity and rotational acceleration under sine curve.**

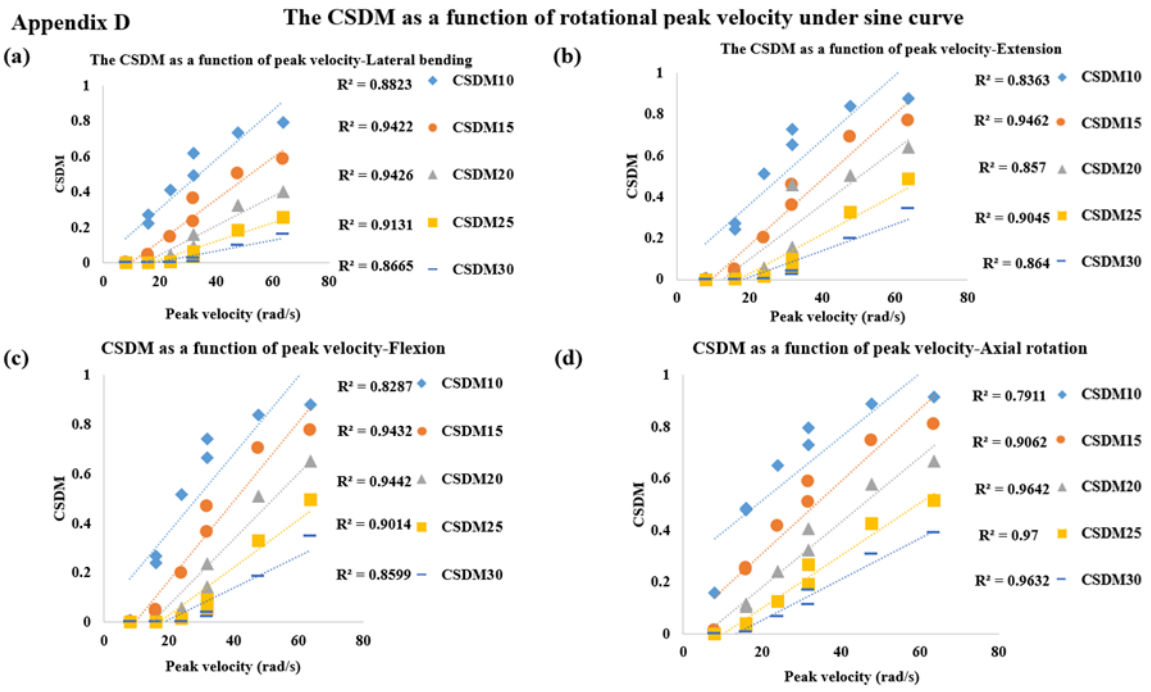


**Figure D.1 The CSDM as a function of peak rotational velocity.**

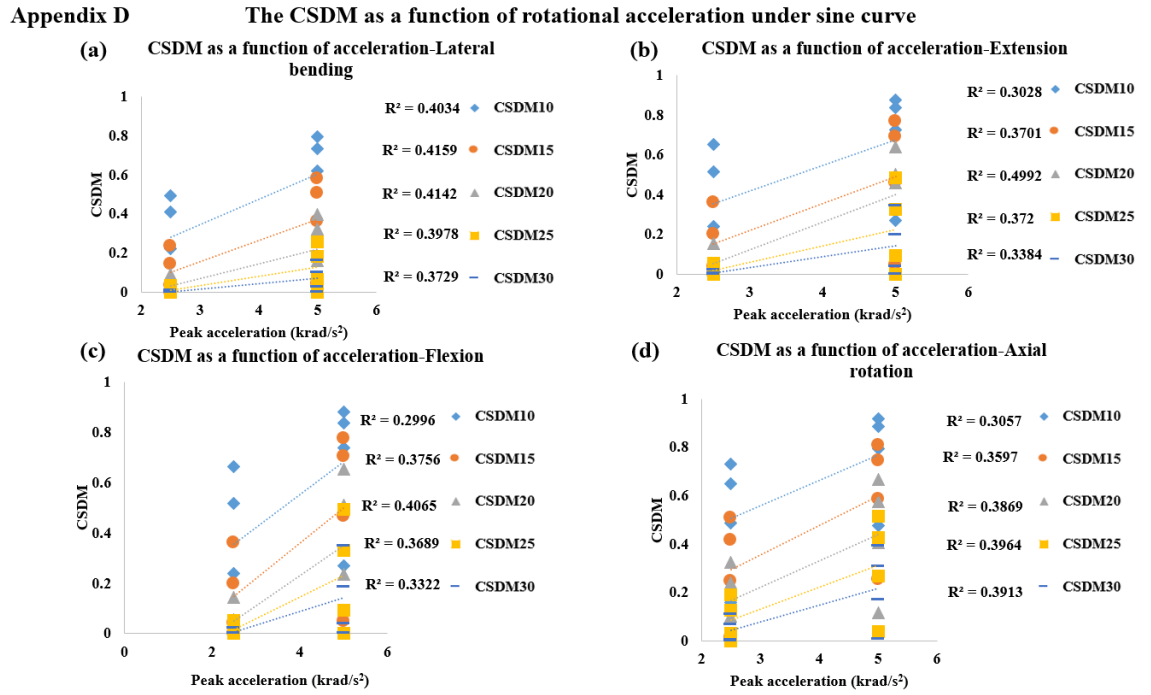


**Figure D.2 The CSDM as a function of rotational acceleration.**

## Appendix E CSDM20 of bare head, head with and without facemask

**Appendix E**

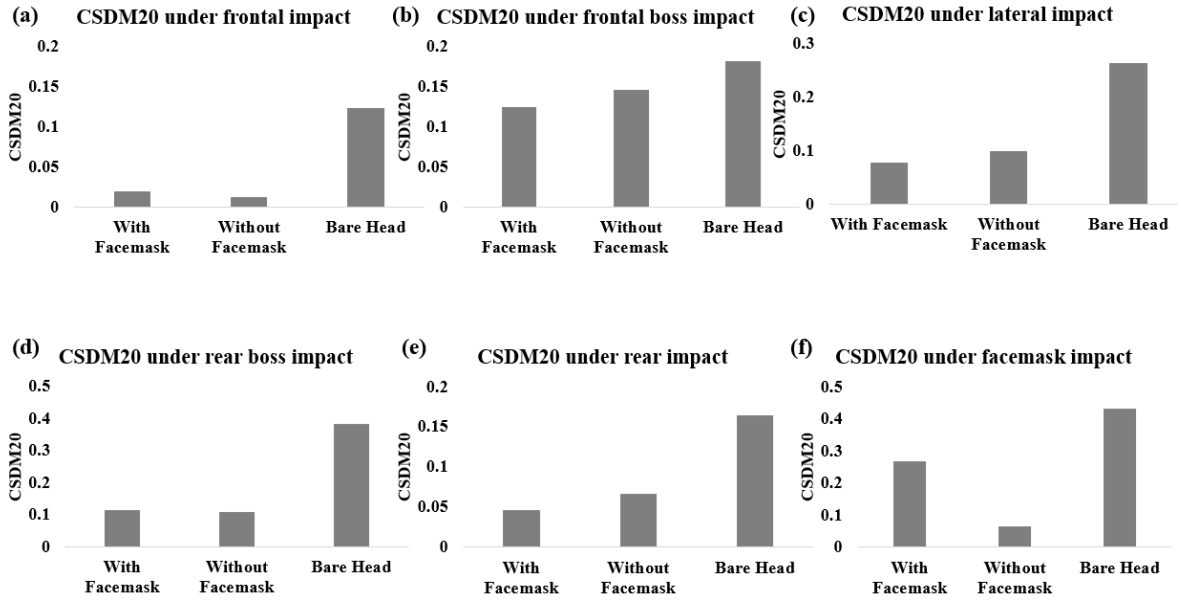


**Figure E.1 CSDM20 of bare head, head with and without facemask**

# Curriculum Vitae

**Name:** Kewei Bian

**Post-secondary Education and Degrees:**
Zhejiang University City College
Hangzhou, Zhejiang, China
2011-2015 B.Eng.

Western University
London, Ontario, Canada
2016-2017 M.Eng.

Western University
London, Ontario, Canada
2017-2019 M. E. Sc

**Honors and Awards:**
2nd Prize of College Students' Comprehensive Abilities in Zhejiang Province
2012-2013

1st Prize of Academic Innovation Team in School of Engineering in Zhejiang University City College
2012-2013

**Related Work Experience**
Teaching Assistant
Western University
2017-2019

**Publications:**

Mao H, Lu L, Bian K, et al. Biomechanical analysis of fluid percussion model of brain injury[J]. Journal of biomechanics, 2018, 77: 228-232.

Bian K, Mao H. Analyzing head-neck tissue strains during football-related impacts[C]//Brain Injury. 2-4 Park Square, Milton Park, Abingdon OR14 4RN, Oxon, England: Taylor & Francis LTD, 2019, 33: 285-286.

Levy Y, Bian K, Mao H. Predicting cognitive impairment following traumatic brain injury: a mathematical approach[C]//Brain Injury. 2-4 Park Square, Milton Park, Abingdon OR14 4RN, Oxon, England: Taylor & Francis LTD, 2019, 33: 291-291.

Bian K, Mao H. Impact directions affect the whole brain and deep brain in different ways[C]//Journal of neurotrauma. 140 Huguenot Street, 3RD FL, New Rochelle, NY 10801 USA: Mary Ann Liebert, INC, 2018, 35(16): A106-A106.

Bian K, Mao H. A comprehensive investigation of the correlation between head rotation and brain strain [J], Submitted in Journal of Biomechanics and Modeling in Mechanobiology.